AN ABSTRACT OF THE THESIS OF

DAVID ARTHUR EMILIA (Name) for the DOCTOR OF PHILOSOPHY (Degree)

in GEOPHYSICS (Major) presented on December 16, 1968 (Date)

Title: NUMERICAL METHODS IN THE DIRECT INTERPRETATION OF MARINE MAGNETIC ANOMALIES

Redacted for Privacy

Abstract approved Professor Gunnar Bodvarsson

Direct interpretation methods for determination of source rock magnetization on the basis of n observed magnetic field values are developed and applied to marine magnetic data. A two-dimensional source body of specified geometry is assumed to consist of n uniformly magnetized volume elements. The equations to be solved are Fredholm integral equations of the first kind. These are numerically approximated by an n x n system of linear algebraic equations which is solved by the method of iteration. The overdetermined problem, where the number of field input points (m) is greater than the number of magnetic volume elements (n), has also been investigated. This is done on the basis of the three approximation norms L_1, L_2, and L_∞. The L_2 norm is best suited to the problem under consideration here.

Application of the direct method to the two-dimensional magnetic

anomalies associated with ocean floor spreading indicates that the magnetization values at the ridge crest are only slightly greater than those away from the crest. This, together with the evidence for narrow transition zones between sections of normal and reverse polarity, lends support to the so called dike injection mechanism for bringing mantle material to the surface at the ridge crest.

Ocean floor spreading rate curves based on the usual associations of magnetic anomalies with the paleomagnetic time scale have been constructed. Two different interpretations appear possible: (1) Spreading rates have been non-uniform along the whole mid-ocean ridge system, and have changed in the same way and at the same time during the past 3.32 my. (2) Spreading rates have been nearly uniform; under this hypothesis, the anomaly usually associated with the Olduvai event should be associated with the Gilsa event, and another anomaly, called W, should be associated with the Olduvai event. The latter interpretation is more acceptable.

Numerical Methods in the Direct Interpretation of Marine Magnetic Anomalies

by

David Arthur Emilia

A THESIS

submitted to

Oregon State University

in partial fulfillment of
the requirements for the
degree of

Doctor of Philosophy

June 1969

APPROVED: Redacted for Privacy

Professor of Geophysics and Mathematics

in charge of major

Redacted for Privacy

Chairman of Department of Oceanography

Redacted for Privacy

Dean of Graduate School

Date thesis is presented December 16, 1968

Typed by Clover Redfern for David Arthur Emilia

ACKNOWLEDGMENTS

This research was performed under the direction of Professor Gunnar Bodvarsson. I am grateful to Professor Bodvarsson for his assistance in selecting this project and for the many helpful suggestions he offered while it was being carried out.

The conversation I had with Professor M. H. P. Bott while visiting England was very interesting and I thank him for giving so freely of his time on that occasion.

Without the aid of Dr. Donald A. Pierce and Mr. Lynn H. Scheurman of the Statistics Department, Oregon State University, the method of linear programming could not have been an integral part of this thesis. Their willingness to consult with me was great, and in turn it is greatly appreciated.

Dr. Donald F. Heinrichs reviewed the interpretation section of this thesis; discussions with him were rewarding and many of his helpful comments were adopted. Professor Tjeerd H. van Andel, Dr. G. Ross Heath, and Dr. Ted C. Moore also made valuable suggestions on this section towards the beginning of this study, and their enthusiasm towards my work was very encouraging.

I would like to acknowledge the pleasant working relationship I had with Dr. Joseph W. Berg, now Executive Secretary of the Earth Sciences Division of the National Academy of Sciences in Washington,

D. C. From July 1965 to June 1967 Dr. Berg was my Major Professor, and the insights into science that I received from him during that period will not be forgotten.

Special thanks are due to Walter M. Pawley for his expertise in computer science, his excellent grasp of numerical methods, and his friendship.

The prayers and encouragement of my parents could never be sufficiently acknowledged here.

The Office of Naval Research sponsored this work under contracts Nonr 1286(10) and Nonr 1286(9), project NR 083-102. From September 1966 to September 1968 I was a recipient of a National Aeronautics and Space Administration fellowship. For this assistance I am grateful.

TABLE OF CONTENTS

LIST OF FIGURES

NUMERICAL METHODS IN THE DIRECT INTERPRETATION OF MARINE MAGNETIC ANOMALIES

INTRODUCTION

For both economic and scientific reasons one of the most important geophysical parameters is the earth's magnetic field. However, until only recently extensive magnetic surveys were not feasible because of the technological difficulties involved in performing such projects. Now, with the development of reliable, easy to operate magnetometers and precise navigation systems the surveyed portion of the earth's surface is increasing rapidly, especially over the world ocean. The need for efficient, easy to apply methods of interpretation of these measurements is a direct product of the increased amount of data. We hope to serve this need by presentation of some methods for the direct determination of magnetization distributions across two dimensional magnetic bodies.

The total magnetic field observed at the surface of the earth represents a combination of the main geomagnetic field, which is believed to originate in the earth's core, and the more localized fields due to magnetic bodies located within the earth's crust. These latter fields, called magnetic anomaly fields, or just magnetic anomalies, are of interest here. Throughout this paper the main geomagnetic field will not be explicitly considered.

Marine Magnetic Anomalies

Of all the magnetic anomalies that exist over the world ocean the most interesting and important, in a megageophysical sense, are those found over the mid-ocean ridge system. In almost every region where this approximately 70, 000 km long system has been surveyed the magnetic anomalies have similar characteristics. They trend parallel to the ridge crest for thousands of kilometers and are nearly symmetrical about that crest for hundreds of kilometers on either side; the largest anomalies are usually found over the ridge crest. The first evidence that this type of anomaly existed over the ocean was presented by Mason (1958), Vacquier, Raff, and Warren (1961), Mason and Raff (1961), and Raff and Mason (1961).

A recent series of papers from the Lamont Geological Observatory (Pitman, Herron and Heirtzler, 1968; Dickson, Pitman, and Heirtzler, 1968; Le Pichon and Heirtzler, 1968; Heirtzler, et al., 1968) has further demonstrated the symmetric and parallel nature of the anomaly pattern. These authors conclude that this pattern may be simulated in each region by the same sequence of two-dimensional source blocks which comprise a series of alternate strips of normally and reversely magnetized material, presumably basalt.

Geological and Geophysical Significance

World wide similarity of the magnetic anomaly pattern over the mid-ocean ridge system suggests that knowledge of the causes of these anomalies may be a very useful aid in reconstruction of the earth's geologic history. With this in mind various authors have presented quite different theories as to the origin of the pattern. Mason and Raff (1961) interpreted the linear pattern off the west coast of the United States in terms of three geological possibilities: (1) isolated bodies of magnetically anomalous material imbedded in non-magnetic material; (2) elevated folds or fault blocks of the main crustal layer; and (3) zones of intrusion of highly magnetic material from the mantle, extending from top to bottom of the crust. Objections have been raised to all three of these possibilities on the grounds of lack of topographic and seismic expression.

Vine and Matthews (1963) have suggested that the regular magnetic anomaly pattern may be due to systematic polarity changes of the remanent magnetization of rocks in the ocean crust. Their interpretation is based on the concept of ocean floor spreading and its possible genetic relation to the anomaly pattern suggested by Dietz (1961). They hypothesize that as the ocean floor is forced apart at the ridge axis by a rising, large-scale, thermal convection current new basaltic material rises nearer to the surface, cools through its Curie temperature, and acquires a thermoremanent magnetization in the direction

of the ambient magnetic field. As the earth's field reverses polarity and the older material moves away from the axis, alternate bands of normally and reversely magnetized material are produced. This in turn leads to alternate bands of positive and negative magnetic anomalies; if the rate of spreading varies in the same manner on both sides of the ridge axis then the anomaly pattern will be parallel to, and symmetric about, that axis. This is in good accordance with the recent discovery of almost periodical polarity changes of the geomagnetic field using radiometric dating in conjunction with paleomagnetic data (Doell, Dalrymple, and Cox, 1966; Doell and Dalrymple, 1966).

Serious objections to the feasibility of the type of currents necessary to cause ocean floor spreading have been raised. Knopoff (1964) concludes that the inhomogeneity in Bullen's region C is amply strong enough to prevent large-scale (mantle-wide) convection from occurring, whether the inhomogeneity involves a phase transition or represents a chemical inhomogeneity. MacDonald (1965) emphasized that large-scale (mantle-wide) convection cells could not maintain the deep structure of continents suggested by heat flow and gravity data.

In contrast to the large-scale convection current mechanism of Dietz for ocean floor spreading, Morgan (1968) and Le Pichon (1968) consider the earth's surface to be made of a number of rigid lithosphere blocks, each bounded by rises, trenches or young fold

mountains, and great faults. These blocks move with respect to one another, thus causing new material to be brought to the surface (at the rises) and older material to be submerged and/or deformed at the trenches or young fold mountains. The source bodies causing the magnetic lineations are formed when dikes are injected into the space left when two blocks spread apart. The mechanism of ocean floor spreading at the mid-ocean ridges, then, corresponds to the breaking apart along lines of weakness of a thick plate in response to some underlying stress pattern. Isacks, Oliver and Sykes (1968) present seismic evidence in favor of the above "block tectonic" theory. They also speculate that the basic driving mechanism for this process is gravitational instability resulting from surface cooling and hence a relatively high density of near-surface mantle materials. Thus, convective circulation in the upper mantle might occur when thin blocks of lithosphere (0-100 km) slide laterally over large distances as they descend; a compensating return flow then takes place in the asthenosphere (100-700 km). Alternatively, they suggest that the surface movement might be taken as the response of the strong lithosphere to relatively simple convection patterns within the weak asthenosphere. The reader is referred to Elsasser (1967) for a discussion of theoretical points pertinent to this problem.

The above mechanisms of Dietz (1961) and Morgan (1968) are dynamic and require large scale earth movement. Other authors

have suggested in situ formation of the magnetic lineations. Ozima, Ozima, and Kaneoka (1968) concluded that the ages of submarine rocks taken from seamounts along magnetic lineations in the western Pacific do not seem to resemble the values expected from the ocean floor spreading hypothesis. However, because of the ambiguity in assigning K-Ar ages of seamounts to the ocean floor and some experimental uncertainties due to the alteration of samples, they do not rule out the possibility of ocean floor spreading. An alternate explanation of the magnetic anomaly lineation pattern can be based on a peculiar property of oceanic basalts which they report to have observed. If one assumes that original oceanic crust consisted of these ocean type basalts and that parts of this original crust were later heated above a certain limit of temperature, then these crustal sections will become more magnetic than continental basaltic sections undergoing the same process. Thus, if hot vapor or lava emanates along regular nets of fissures or ocean ridge fractures, then regular magnetic anomaly patterns would be formed. The density and seismic velocity of the basalts would not be affected by this process and therefore, seismic and gravity measurements would not indicate any difference between the original crust and the heated area. The basalts may be more magnetic along the ridge axis, where the highest temperature is reached, and roughly bilaterally symmetrical magnetic anomaly patterns may be obtained.

In another recent paper van Andel (1968) presents a mechanism for the in situ formation of the magnetic lineations which assumes arching of a pre-existing crust, and which satisfies various geologic conditions. This arching, possibly due to thermal expansion or hydration of the underlying mantle, could result in a broad zone of tensional fracturing with dike formation and outflow of plateau basalts. Progressive consolidation of the crust, following upwarping, would proceed inward from the margins of the arch, leaving behind a symmetric pattern of positive and negative magnetic anomalies and leading to a gradual narrowing of the volcanic belt.

Vine and Tuzo Wilson (1965) compared the measured anomaly field across the Juan de Fuca Ridge with the fields of various two-dimensional magnetization distributions that may result from the dynamic process of ocean floor spreading. They found that the higher frequencies of the measured anomaly could not be generated by a simple block model extending from the top to the bottom of the crust (3-11 km), but the assumption of such a model located within the second oceanic layer (3.3-5 km) significantly improved the fit. For the same profile Bott (1967) directly calculated the two-dimensional magnetization distribution of bodies similar to those considered by Vine and Tuzo Wilson. He concluded that excessively strong magnetization contrasts are required by a body located within the third oceanic layer (5-11 km) and that the measured anomaly can be reasonably explained

by a body within, or partly within, the second layer.

The conclusions of Vine and Tuzo Wilson and Bott are in good accord with the theory of Hess (1965) that basalt accounts for only a thin veneer one or two kilometers thick on top of a main crustal layer of serpentinite which is virtually non-magnetic. Hess postulates that the generation of this basalt may result from some pressure-sensitive separation process being applied to a rising column of hot-mantle peridotite; this basalt reaches the surface through fissure eruptions. Hydration of remaining mantle material then leads to the serpentinite layer comprising the largest portion of the oceanic crust (layer 3).

There is a large amount of observational evidence supporting the theory that all linear magnetic anomalies parallel to the mid-ocean ridge axis are due to ocean floor spreading occurring contemporaneously with geomagnetic field reversals. This view will be adopted here and our ultimate conclusions are based on its validity. If, however, this theory is at some time completely disproved and/or some other theory is shown to be more feasible, then the conclusions in this paper may not be applicable.

From the above discussion then, the following working model is to be used in the interpretation of these anomalies: The source body is two-dimensional and lies parallel to the trend of the magnetic anomaly pattern. It is two kilometers thick with the upper surface

located just under the ocean bottom and both the upper and lower surfaces slope away from the ridge crest in the same manner as the general topography. The average configuration of the paleo-geomagnetic field is assumed to be that of an axially symmetric dipole, and therefore the direction of magnetization in the source body is chosen to be as if the magnetization was induced by such a field.

Methods of Interpretation

The problem of magnetic field interpretation in geophysics consists of finding the distribution of magnetic material whose magnetic field is given on a plane surface. Unfortunately, this problem has a unique solution only when the field is given throughout the body. This is evident from Poisson's equation which gives the relation of the magnetic field over all space to the source distribution of magnetization:

$$\nabla^2 A = -4\pi \nabla \cdot \vec{M}$$

$$\Delta \vec{H} = -\nabla A,$$

where A is the scalar magnetic potential throughout all space, $\Delta \vec{H}$ is the complete magnetic anomaly field throughout all space, and $\vec{M}$ is the vector magnetization distribution in the source body. The solution of A in terms of $\vec{M}$ is given below by Equation (1), and the reader is referred there and to Grant and West (1965) for a more

complete discussion of the potential theory.

The lack of uniqueness, or the ambiguity of the problem of magnetic field interpretation can also be seen from the fact that a finite number of parameter functions are involved in describing a source distribution, and an infinite number of combinations of these can produce the same field configuration in the limited region under consideration. However, even though no unique solution is possible, the range of acceptable solutions is limited by physical considerations. For example, the Curie temperature puts an upper limit on the depth in the earth at which a body can lie (usually around 25 km), the magnitude of the computed magnetization should not greatly exceed any directly measured values, and the magnetization should be a reasonably smooth function of position.

Specific factors which contribute to the ambiguity of the magnetic problem are errors in measurements due to time variations of the geomagnetic field, navigational errors, data reduction errors, and instrument error. Interference from neighboring bodies can greatly alter the true form of the subject anomaly, and disparity between model and reality can be a serious source of ambiguity for both qualitative and quantitative interpretation. In practice, then, only a limited amount of information can be obtained about the true source body; some of the body parameters must be assumed, and the remaining parameters must be either directly or indirectly estimated to

within the accuracy of the observed anomaly.

Various methods of magnetic interpretation have been developed for different purposes. Peters (1949) derives approximate methods for the direct determination of basement structure. Vacquier, et al. (1951) interpret total intensity maps with the help of three-dimensional (prismatic) bodies and computed second derivatives. Smellie (1956) gives total intensity depth factors for point and line configurations of poles and dipoles, and Smith (1959, 1961) derives inequalities which can be used to estimate the depth and intensity of magnetization for arbitrary bodies. Heirtzler, et al. (1962) give sets of model anomalies with rules for depth determinations. Bott, Smith, and Stacey (1966) describe a method for determining the direction of magnetization of a body causing a magnetic anomaly, and Bott (1967) gives a method for direct determination of the magnetization distribution in a two-dimensional body of rectangular cross section. There are, of course, many other pertinent papers that could be mentioned here and the reader is referred to Heirtzler, et al. (1962) for an extensive bibliography on magnetic interpretation methods prior to that time.

THE DIRECT METHOD OF INTERPRETATION

In the previous section some direct methods of interpretation of magnetic anomalies were mentioned. By definition, this implies direct use of the measured anomaly field to determine some physical parameter pertaining to the anomaly source. In the indirect method of interpretation anomalies are computed for trial bodies and these are compared to the observed anomalies; on the basis of this comparison the physical distribution under consideration is then adjusted so that the fit of the computed anomaly to the observed anomaly is improved.

Comparison with the Indirect Method

Both the direct and indirect methods have their advantages and disadvantages, and some of these will be listed here. Let it first be noted, however, that throughout the remainder of this paper discussion will be confined to determination of the magnetization distribution of a source body given the size, shape, and location of the body and the direction of magnetization.

Advantages of the indirect method: The fields due to very extensive horizontal and vertical distributions of magnetization and complex source configurations can be calculated handily on existing computers. Mathematical analysis is quite straightforward; computer

programs that are relatively easy to apply are available in the literature (Heirtzler, et al., 1962; Talwani and Heirtzler, 1964).

Disadvantages of the indirect method: A complete magnetization distribution must be assumed, thus adding to the already long list of assumptions. This distribution must be adjusted after each trial calculation so that the computed anomaly will give a better fit to the observed anomaly; no formal criterion exists for adjustment of the subsequent magnetization distributions, and formal criteria are very seldom used for determining how well the computed anomaly fits the observed anomaly. This can be very important in detailed work. Also, because of the necessity of assuming the magnetization distribution, much of the detail of large problems may tend to be neglected.

Advantages of the direct method: The magnetization distribution is calculated explicitly and no subsequent arbitrary adjustments need be made. The detail of the analysis depends on the number of input points (observed anomaly in digitized form) and on the number and size of the intervals over which the magnetization is calculated. Thus one does not have to make complex assumptions in order to obtain details. Direct solution by the method of iteration, or other approximate methods, allows the magnetization to be estimated to just within the accuracy warranted by the measurement accuracy of the anomaly field. Direct solution by linear programming allows investigation of the response of the system to slight changes in the assumed

parameters without having to re-run the entire problem. With linear programming it is also possible to take into consideration any statistical fluctuations of the system parameters when the probability distributions of these fluctuations are known (Garvin, 1960).

Disadvantages of the direct method: The observed anomaly must be digitized. A vertical distribution of magnetization can be treated only in a limited sense. Mathematical (numerical) analysis can be quite involved and problems take more computer time than with the indirect method (assuming only a few distribution adjustments in the latter are necessary). For relatively large problems the linear programming method of direct solution is possible only on large computers; complete linear programming packages are very difficult to write and are not readily available.

Analytical and Numerical Discussion of the Direct Problem

Let us now consider more rigorously the problem of determining the magnetization distribution when the size, shape, and location of the source body and the direction of magnetization are known.

The scalar magnetic potential at an external point due to a volume of material which is magnetized with a magnetization $\vec{M}$ is

$$(1) \qquad A(\vec{r}_P) = \int_V \vec{M}(\vec{r}_Q) \cdot \nabla_Q \frac{1}{|\vec{r}_P - \vec{r}_Q|} \, d\vec{r}_Q \, .$$

Hence the vector $\vec{r}_P$ describes the position of the point of observation with respect to the origin and the vector $\vec{r}_Q$ describes the position of a point in the body under consideration (Figure 1).

The intensity of the magnetic field at the point $\vec{r}_P$ is given by the negative gradient of $A(\vec{r}_P)$. Since this is an anomalous magnetic field superimposed on the regional geomagnetic field the complete anomaly field $\Delta\vec{H}$ is written

$$\Delta\vec{H}(\vec{r}_P) = -\nabla_P A(\vec{r}_P).$$

Now assume that the anomaly field is much less than the regional geomagnetic field (as is almost always the case). Then the component of the anomaly field measured by a total-field magnetometer is that which lies in the direction of the regional geomagnetic field (Grant and West, 1965). This component, called $\Delta T(\vec{r}_P)$, is written

$$\Delta T(\vec{r}_P) = -\frac{\partial}{\partial \hat{t}} A(\vec{r}_P) \tag{2}$$

where $\hat{t}$ signifies the direction of the regional geomagnetic field (Figure 2a).

Let the direction of $\vec{M}(\vec{r}_Q)$ be defined by the unit vector $\hat{s}$ (Figure 2b). Then the vector operation $\vec{M}(\vec{r}_Q) \cdot \nabla_Q$ in Equation (1) can be written as $M(\vec{r}_Q)\frac{\partial}{\partial \hat{s}}$.

From the above discussion the expression for a total-field

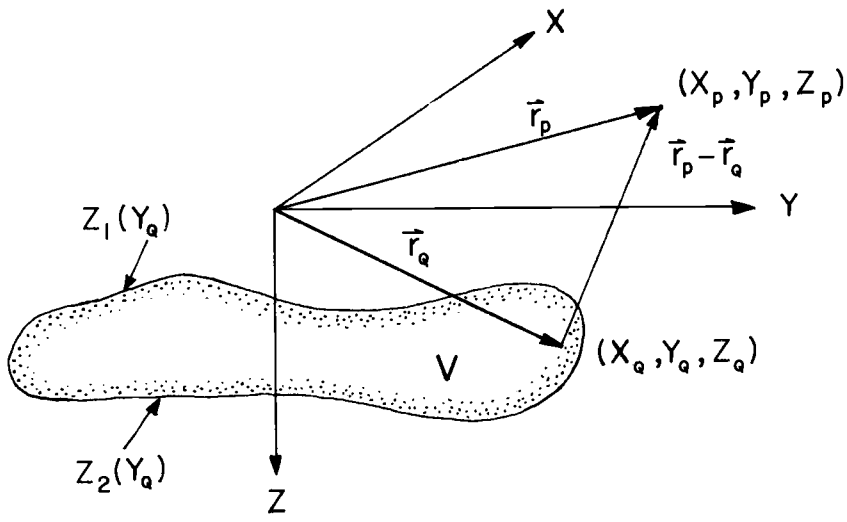

Figure 1. Coordinate system used in this paper. $\vec{r}_P$ describes the point of observation and $\vec{r}_Q$ describes a point in the body under consideration. Only bodies infinite along the x-axis are considered.

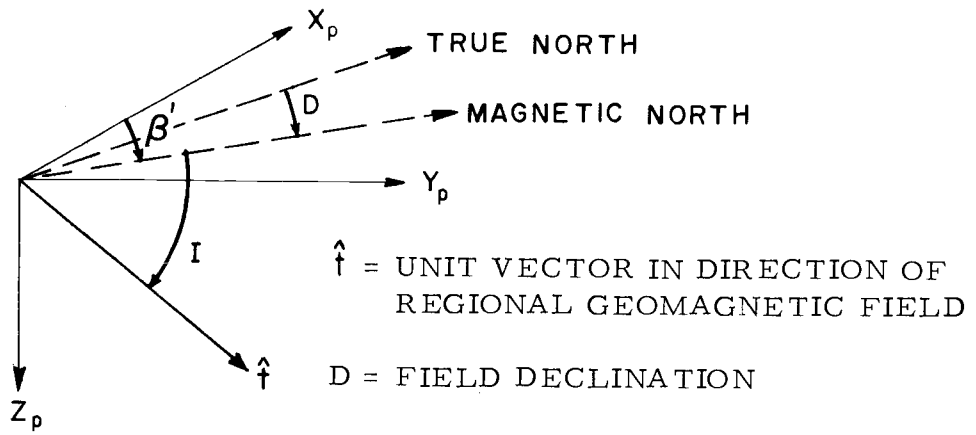

$$\frac{\partial}{\partial \hat{t}} = \cos I \cos \beta \frac{\partial}{\partial X_p} + \cos I \sin \beta \frac{\partial}{\partial Y_p} + \sin I \frac{\partial}{\partial Z_p}$$

(a)

Figure 2(a). Parameters describing the direction of the regional geomagnetic field.

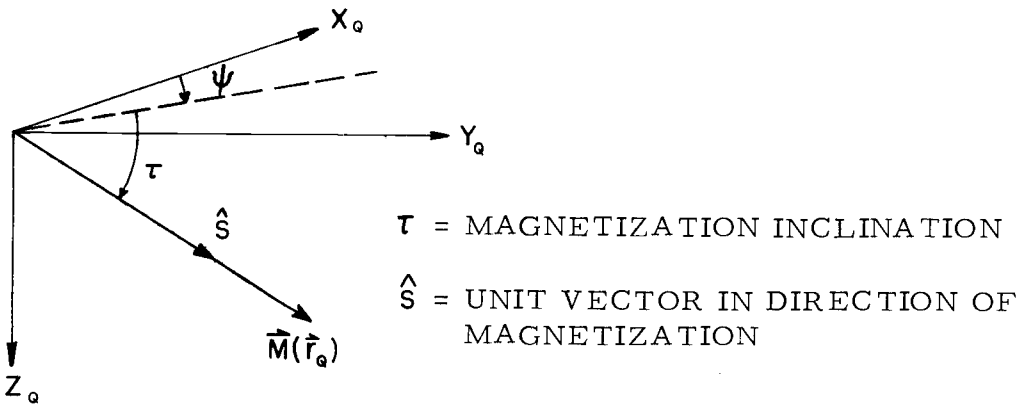

$$\frac{\partial}{\partial \hat{s}} = \cos \tau \cos \psi \frac{\partial}{\partial X_Q} + \cos \tau \sin \psi \frac{\partial}{\partial Y_Q} + \sin \tau \frac{\partial}{\partial Z_Q}$$

(b)

Figure 2(b). Parameters describing the direction of the magnetization.

magnetic anomaly is

$$(3) \qquad \Delta T(\vec{r}_P) = -\frac{\partial}{\partial \hat{t}} \int_V M(\vec{r}_Q) \frac{\partial}{\partial \hat{s}} \frac{1}{|\vec{r}_P - \vec{r}_Q|} \, d\vec{r}_Q .$$

The anomalies associated with ocean floor spreading can be considered to be caused by two-dimensional bodies of finite depth extent. In this paper each anomaly of this type is treated as a profile along the y_P axis, perpendicular to the strike of the body. The $z_P = 0$ plane is the surface of observation and the z coordinate is positive downwards (Figure 1).

With the above restrictions, and after some manipulation, Equation (3) becomes

$$(4) \qquad \Delta T(y_P) = \int_a^b M(y_Q) G(y_P - y_Q, z_1(y_Q), z_2(y_Q)) dy_Q$$

where:

a and b define the limits of the source body in the y direction, $z_1(y_Q)$ and $z_2(y_Q)$ are its upper and lower surfaces respectively,

$$(5) \qquad G = (z_2 - z_1) \left\{ \frac{-c_1 y_{PQ}^2 + c_2 (z_2 + z_1) y_{PQ} + c_1 z_1 z_2}{(y_{PQ}^2 + z_1^2)(y_{PQ}^2 + z_2^2)} \right\} ,$$

$$c_1 = 2(\sin\tau \sin I - \cos\tau \sin\psi \cos I \sin\beta'),$$

$$c_2 = 2(\sin\tau \cos I \sin\beta' + \cos\tau \sin\psi \sin I),$$

$$y_{PQ} = y_P - y_Q.$$

The kernal is represented as G because it is a function of the geometry of the body.

Thus, the problem of direct determination of the magnetization distribution reduces in this case to the problem of solving the above integral equation for $M(y_Q)$. The kernal G is square integrable and bounded, and Equation (4) is called a Fredholm integral equation of the first kind.

Formal solution of Equation (4) can be obtained in terms of the eigenfunctions $(f_r(y_P))$ and eigenvalues $(\lambda_r \neq 0)$ of the kernal $G(y_P, y_Q)$. More explicitly, suppose that $\Delta T(y_P)$ can be expanded as a linear combination of $f_r(y_P)$; then

$$\Delta T(y_P) = \sum_r a_r f_r(y_P),$$

and the solution of Equation (4) is (Fox, 1962)

$$M(y) = \sum_r \frac{a_r}{\lambda_r} f_r(y) \quad (\lambda_r \neq 0). \tag{6}$$

Solution in this manner is impractical because of the difficulty of

finding the eigenvalues and the necessarily complete set of eigenfunctions. It is also clear from Equation (6) that the formal method breaks down not only when certain eigenvalues are identically zero, but when $\lambda_r \to 0$ much faster than a_r.

Since Equation (4) will eventually have to be solved numerically the above considerations must be stated in the language of numerical analysis. Numerical representation of Equation (4) yields the matrix equation

$$G\vec{M} = \Delta\vec{T} \tag{7}$$

where G is the square $(n \times n)$ matrix, $\Delta\vec{T}$ is the vector whose n components are the measured values of $\Delta T(y_P)$, and $\vec{M}$ is the vector whose n components are the unknown values of $M(y_Q)$ over specified intervals. We therefore wish to discuss the relations of the eigenvalues $(\mu_1, \ldots, \mu_n)$ and the eigenvectors $(\vec{g}_1, \ldots, \vec{g}_n)$ of G to the solution $\vec{M}$. That is, $\Delta\vec{T}$ can now be expanded in terms of the eigenvectors $\vec{g}_i$:

$$\Delta\vec{T} = \sum_{i=1}^{n} b_i \vec{g}_i ,$$

and the equation

$$\vec{M} = \sum_{i=1}^{n} \frac{b_i}{\mu_i} \vec{g}_i \qquad (u_i \neq 0)$$

is the numerical equivalent to Equation (6).

This expansion is only an approximation to Equation (6) and it is obvious that small errors in b_i, corresponding to small μ_i, have big effect on the solution. The problem of solving Equation (7) may then be ill-conditioned (unstable) in the sense that slight perturbations to the left side (G) and/or the right side ($\Delta\vec{T}$) may result in large perturbations to the solution ($\vec{M}$). In practical applications these slight perturbations usually take the form of computer roundoff errors, and in terms of Equation (7) their possible effect can be visualized by the relations

$$(G+\delta G)(\vec{M}+\delta\vec{M}) = \Delta\vec{T} + \delta\Delta\vec{T}$$

or

$$\delta\vec{M} = (G+\delta G)^{-1}(\delta\Delta\vec{T}+\delta G\vec{M})$$

where δ represents a perturbation.

Initially suppose that G is treated exactly ($\delta G=0$), but that $\Delta\vec{T}$ is subject to roundoff uncertainty. Then

$$\delta\vec{M} = G^{-1}\delta\Delta\vec{T}$$

where G^{-1} is the matrix inverse to G. In terms of vector and matrix norms, as defined in Forsythe and Moler (1967), the last equation is

$$\|\delta\vec{M}\| \leq \|G^{-1}\| \cdot \|\delta\Delta\vec{T}\|.$$

Multiply this by $\|\Delta\vec{T}\| \leq \|G\| \cdot \|\vec{M}\|$ and rearrange to get

$$\frac{\|\delta\vec{M}\|}{\|\vec{M}\|} \leq \|G\| \cdot \|G^{-1}\| \cdot \frac{\|\delta\Delta\vec{T}\|}{\|\Delta\vec{T}\|}$$

That is, for any nonsingular matrix G the condition number, defined as

$$\text{cond}\,(G) = \|G\| \cdot \|G^{-1}\| \geq 1,$$

bounds the relative uncertainty of the solution $\vec{M}$ to that of the given $\Delta\vec{T}$ (Forsythe and Moler, 1967). The condition number is invariant when G is multiplied by a constant, and various authors (Turing, 1948; Faddeev and Faddeeva, 1963; Forsythe and Moler, 1967) point out that it is a reasonably good measure of the instability of a system. If indeed cond (G) is large, then small perturbations in $\Delta\vec{T}$ may greatly alter $\vec{M}$. This alteration usually takes the form of high amplitude, high frequency noise superimposed on the desired solution. Much has been written in the literature (Bullard and Cooper, 1948; Kreisel, 1949; Phillips, 1962; Baker, et al., 1964) concerning ways to separate out this noise. All methods involve a smoothing process of one form or another applied either to the input data or the output data.

The possible high sensitivity of $\vec{M}$ to slight perturbations of

the elements of G is quite evident if it is realized that although the analytical form of G is known (Equation (5)), the numerical values of its elements are not known exactly and obviously must be rounded off in the computer. In discussing the effect of this characteristic of G on the final solution we refer to the excellent section on conditioned matrices of Faddeev and Faddeeva (1963).

Formal solution of Equation (7) is given by the expression

$$\vec{M} = G^{-1}{}_{\Delta}\vec{T}$$

This expression suggests that the sensitivity of $\vec{M}$ to small changes in the elements of G may ultimately be discussed in terms of the sensitivity of the elements of G^{-1} to small changes in the elements of G. It is well known that G^{-1} exists if, and only if, the determinant of G is non-zero. For cases where the exact determinant is only slightly different from zero, the computer roundoff can sufficiently change the elements to lead to a matrix with determinant equal to zero! That is, small perturbations in the elements of a matrix may equivalently lead to very large changes in the elements of its inverse. If this happens, the matrix is said to be unstable or ill-conditioned.

However, it is not to be concluded from the above discussion that the determinant of a matrix is an indication of the stability of its inverse, and that a small determinant means an unstable system. In

many cases the determinant is not a reliable indication of the stability of a system; for example, it is obvious that the matrices G and (const) $\cdot$ G should be considered equally stable, but their corresponding determinants will be different. Matrix stability must therefore be characterized by a quantity independent of constant factors in the matrix and, it might be added, independent of the dimensions of the matrix. Forsythe and Moler (1967) point out that this quantity is the condition number of the matrix G in the sense that

$$\frac{\|\delta\vec{M}\|}{\|\vec{M}\|} \leq \text{cond } (G) \cdot \frac{\|\delta G\|}{\|G\|} \quad \text{(for small } \frac{\|\delta G\|}{\|G\|}\text{)}.$$

It is then clear that cond (G) is generally a reliable indication of the stability of $\vec{M}$ with respect to changes in the elements of G and $\Delta\vec{T}$. Cond (G) greater than about 100 indicates a relatively unstable system (J. Davis, personal communication, 1968). A commonly used condition number is

$$\text{cond } (G) = \|G\| \cdot \|G^{-1}\| = \mu_1/\mu_n \geq 1$$

where μ_1 and μ_n are the largest and smallest eigenvalues of the matrix G (Faddeev and Faddeeva, 1963). This expression supports the previous conclusions that relatively small eigenvalues of G could very likely yield an unstable system. In all the cases (four) tested for anomalies and models associated with ocean floor spreading

the condition numbers of G were less than 10. Thus no corrective measures had to be applied to overcome any effects of ill-conditioned matrices.

It might be asked, however, under what circumstances will matrices of the type under discussion become unstable. The answer lies in a consideration of the physical requirements placed on a system. For example, in every case associated with ocean floor spreading treated here the source body was chosen to have nearly the same dimensions as the magnetic profile, and the position of the center of each magnetic volume element was chosen to correspond closely to the position of a field point. Thus the system was not "forced" to reach a solution. That is, a physically reasonable magnetization distribution was sufficient, and the magnetization values were not sensitive to small changes in the field values. If, however, a source body had been chosen to be much smaller in extent than the profile under consideration, then a solution would be forced. Therefore, small changes in the more distant field values would greatly affect the magnetization values and the system would be highly unstable. This situation is to be avoided by a judicious choice of the relations between model and field parameters.

Methods of Solution

In component form Equation (7) is written

$$\Delta T_j = \sum_{k=1}^{n} G_{jk} M_k \quad (j=1, \ldots, n), \tag{8}$$

and the problem of finding M_k from ΔT_j is that of solving an $n \times n$ system of linear algebraic equations. Many methods of solving such a system are available and the reader is referred to Faddeev and Faddeeva (1963) and Fox (1965) for very comprehensive treatments of this subject. Two methods for determining M_k from Equation (8) will be discussed in this paper; one yields an exact solution (Gaussian reduction) and the other yields an approximate solution (iteration).

Gaussian reduction (or elimination) consists of a chain of successive eliminations which transform the given system of equations into a system with a triangular matrix; the solution of this system is then quite straightforward. A detailed description of the processes involved in this method is given by Fox (1965).

Approximate solution of Equation (8) is obtained by the method of iteration. This approximate solution is the limit of a sequence of certain vectors constructed by a uniform process called the iteration process. For discussion of solution by iteration, Equation (7) is reduced to the form

$$(I-L-U)\vec{M} = \vec{S} \tag{9}$$

where L and U are lower and upper triangular matrices with zero elements along their diagonals, and I is the unit matrix. This form is obtained by dividing each equation in Equation (8) by its diagonal coefficient and expressing the result in matrix form.

In the simplest iteration process, called the process of successive approximations by Faddeev and Faddeeva (1963), sequence vectors are constructed according to the formula

$$\vec{M}^{(i)} = (L+U)\vec{M}^{(i-1)} + \vec{S} \tag{10}$$

where $\vec{M}^{(0)}$ is the initial approximation to $\vec{M}$. Obviously, if the sequence $\vec{M}^{(0)}, \ldots, \vec{M}^{(i)}, \ldots$ can converge to $\vec{M}$ then this limit will be the solution of Equation (9). In this paper, however, we choose to use the Seidel iteration process (Faddeeva, 1959) whereby computation of the sequence vectors is performed by the formula

$$\vec{M}^{(i)} = L\vec{M}^{(i)} + U\vec{M}^{(i-1)} + \vec{S} \qquad (C = L + U) \tag{11}$$

or, in component form

$$M_k^{(i)} = \sum_{j=1}^{k-1} C_{kj} M_j^{(i)} + \sum_{j=k}^{n} C_{kj} M_j^{(i-1)} + S_k. \tag{12}$$

The difference between the Seidel method and the method of successive approximations is that in the latter the complete ith sequence vector is computed before the (i+1)th vector is considered, while

in the former, all the previously computed elements of the ith vector are considered when computing the remaining components of that vector. The Seidel method thus makes maximum use of all available information.

Choice of the initial approximation vector is quite arbitrary, but it is reasonable to choose one as close to the desired solution as possible in order to reduce computation time. From a physical point of view the magnetization along a profile is expected to vary in much the same way as the field; in other words, $\vec{M}$ and $\vec{S}$ in Equation (9) should have similar shapes; this suggests that a physically good choice for $\vec{M}^{(0)}$ is $\vec{S}$. From a computational point of view the choice $\vec{S}$ is also good, because from Equation (10) it is already one iteration step further along than if $\vec{M}^{(0)} = \vec{0}$ had been chosen. Here we have looked to the method of successive approximations for help in choosing a computationally reasonable initial sequence vector, but it is evident from Equation (11) that this vector is also reasonable for use with the Seidel method. Of course, for each specific problem a much better explicit choice of $\vec{M}^{(0)}$ than $\vec{M}^{(0)} = \vec{S}$ can be made, but the personal time and effort involved in repeatedly doing this overcomes any computational time saved.

Till now the question of how to terminate the iteration process has not been discussed. One is free to choose any suitable relation between the kth sequence vector and either the (k-1)th vector,

or the vector $\vec{S}$, or even the vector $\Delta\vec{T}$ as the point in the computation which, when reached, requires the process to be stopped. This criterion may be purely mathematical, or it may have a physical basis. Of the many possible mathematical criteria the easiest and quickest to apply relates $\vec{M}^{(k)}$ and $\vec{M}^{(k-1)}$; that is, the process is stopped when the Euclidean norm of the vector $\vec{M}^{(k)} - \vec{M}^{(k-1)}$ is less than some specified constant times the Euclidean norm of $\vec{M}^{(k-1)}$:

$$\|\vec{M}^{(k)} - \vec{M}^{(k-1)}\|_e < \text{const } \|\vec{M}^{(k-1)}\|_e . \tag{13}$$

The constant factor is to be chosen in view of the particular problem under consideration. As the problem has a physical basis, it is reasonable to want a physical criterion for stopping the iteration process. Obviously, something that gives an approximate solution of only the accuracy warranted by the experimental accuracy of the input field (ΔT_j) is ideal. A stopping norm of the L_∞ type (see the section, The Overdetermined Problem) is found to be best suited to this purpose, and computation is required to stop when

$$\max_j \left|\Delta T_j - \sum_{k=1}^{n} G_{jk} M_k^{(i)}\right| < E \quad (j=1, \ldots, n), \tag{14}$$

where E represents the error from measurement and data

reduction. That is, computation is stopped when the absolute value of the maximum component of the residual vector is less than the estimated error in the input field. Equation (14) is computationally unwieldy and, of course, if the model is poorly chosen it may never be satisfied. In view of these facts, a combination of Equations (13) and (14) should be used in the following manner as a stopping criterion. Both are applied, Equation (14) is tested every second iteration (to reduce computation time), and if Equation (13) is satisfied first the process is stopped; otherwise, the process is stopped when Equation (14) is satisfied.

APPLICATIONS AND DISCUSSION

Up to this point an introduction has been given to the type of magnetic anomaly fields under consideration and possible direct methods to derive the magnetization distributions associated with these anomalies have been derived. In this section we present the working equations by which these methods are to be applied, and the iteration method will be applied to the interpretation of important magnetic anomalies associated with ocean floor spreading.

The Working Equations

We have given Equation (8)

$$\Delta T_j = \sum_{k=1}^{n} G_{jk} M_k \quad (j=1, \ldots, n) \tag{8}$$

as a numerical approximation to Equation (4)

$$\Delta T(y_P) = \int_a^b G(y_P - y_Q, z_1(y_Q), z_2(y_Q)) M(y_Q) dy_Q \, . \tag{4}$$

The working equations are derived from Equation (4) as follows: In approximate form Equation (4) is written

$$\Delta T(y_P) \simeq \sum_{k=1}^{n} M_k \int_{a_k}^{b_k} G(y_P - y_{Qk}, z_{1k}, z_{2k}) dy_{Qk};$$

that is, the field along a profile is the superposition of the fields due to n two-dimensional rectangular volume elements lying side by side perpendicular to that profile, each of preassigned width and uniform magnetization. Upon evaluation of the above integral (see Equation (5) for G) the working equation takes the form

$$10^5 \Delta T_j = \sum_{k=1}^{n} M_k G_{jk} \quad (j=1, \ldots, n)$$

where (at this point the reader should refer to Figure 3)

ΔT_j is the anomaly at the jth field point in gammas (one gamma equals 10^{-5} oersteds),

M_k is the magnetization of the kth volume element in emu/cm^3,

a_k and b_k define the y_Q-dimensions in cm of the kth two-dimensional volume element,

z_{1k} and z_{2k} are the constant depths in cm to the upper and lower surfaces respectively of the kth volume element,

and G_{jk} is the anomaly at the jth field point caused by the kth volume element with $M_k = 1$.

G_{jk} is then expressed by

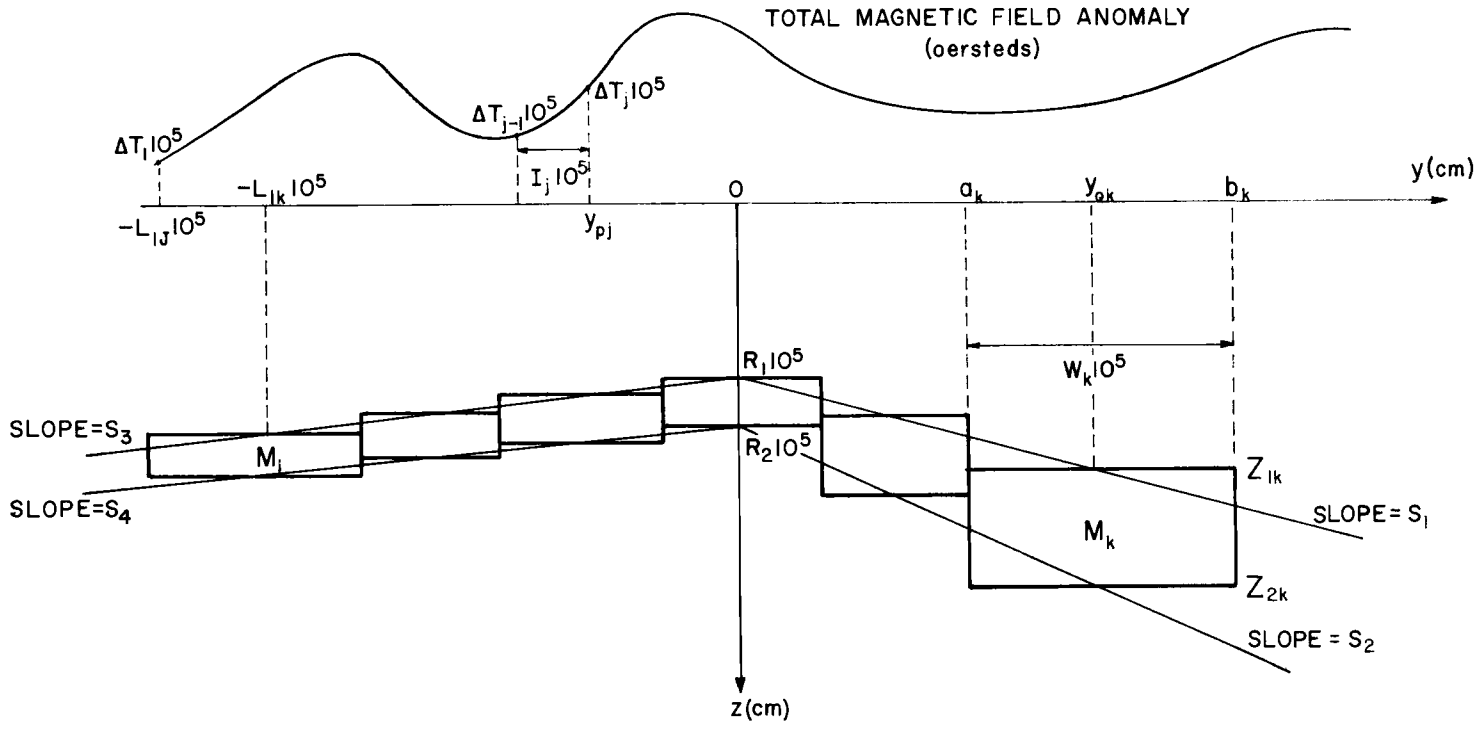

Figure 3. Parameters used in the working equations.

$$G_{jk} = c_1 \left[\tan^{-1} \frac{b_k - y_{Pj}}{z_{1k}} - \tan^{-1} \frac{a_k - y_{Pj}}{z_{1k}} - \tan^{-1} \frac{b_k - y_{Pj}}{z_{2k}} + \tan^{-1} \frac{a_k - y_{Pj}}{z_{2k}} \right]$$

$$+ \frac{c_2}{2} \log_e \frac{[(a_k - y_{Pj})^2 + z_{1k}^2][(b_k - y_{Pj})^2 + z_{2k}^2]}{[(b_k - y_{Pj})^2 + z_{1k}^2][(a_k - y_{Pj})^2 + z_{2k}^2]},$$

where

c_1 and c_2 are given in Equation (5),

y_{Pj} = the dimension in cm describing the position of the jth field point = $[-L_{\ell J} + \sum_{p=2}^{j} I_p] 10^5$,

$-L_{\ell J}$ is the position in km of the first field point to be considered (all other field points are to its right in the direction of increasing y_P),

I_p is the distance in km from the (p-1)th to the pth field point in the direction of increasing y_P,

$$a_k = y_{Qk} - \frac{W_k}{2} 10^5, \quad b_k = a_k + W_k 10^5,$$

y_{Qk} = the dimension in cm describing the position of the center of the kth volume element

$$= [-L_{\ell K} + \frac{\theta_{1k}}{2} (W_1 + W_k + 2 \sum_{p=2}^{k-1} W_p)] 10^5,$$

$-L_{\ell K}$ is the location in km of the midpoint of the first volume element under consideration (all other volume elements are

to its right in the direction of increasing y_Q),

$$\theta_{1k} = \begin{cases} 0, & k = 1 \\ 1, & \text{otherwise,} \end{cases}$$

W_p is the width in km of the pth volume element.

In all applications here the upper and lower surfaces of the two-dimensional source body (described as a function of the midpoints of the volume elements) are required to have constant, but not necessarily equal, slopes on either side of the origin; then z_{1k} and z_{2k} are of the form

$$\left.\begin{aligned} z_{1k} &= 10^5 R_1 + S_1 y_{Qk} \\ z_{2k} &= 10^5 R_2 + S_2 y_{Qk} \end{aligned}\right\} y_{Qk} \geq 0$$

$$\left.\begin{aligned} z_{1k} &= 10^5 R_1 + S_3 y_{Qk} \\ z_{2k} &= 10^5 R_2 + S_4 y_{Qk} \end{aligned}\right\} y_{Qk} < 0,$$

where R_1 and R_2 are the depths to the upper and lower surfaces respectively at the origin, and S_1, S_2, S_3, S_4, are the slopes of the pertinent surfaces.

For each particular problem, then, the following parameters must be specified:

R_1 (km), R_2 (km), S_1, S_2, S_3, S_4, ψ, β', I, τ, n,

$W_1 \ldots W_n$ (km), $I_2 \ldots I_n$ (km), $L_{\ell J}$ (km), $L_{\ell K}$ (km),

$\Delta T_1 \ldots \Delta T_n$ (gammas).

The number of field values, and therefore the digitization interval, used in the working equations must be chosen judiciously. There must be a sufficient density of points to properly describe the desired field information. On the other hand, most magnetic field measurements are made at discrete points, so any digitization interval smaller than the measurement interval would usually be unwarranted.

One of the purposes of the applications in the next section is to distinguish sections of normal and reverse polarity. Therefore, the digitization intervals and widths of the magnetic volume elements must be chosen small enough to allow the smallest section of interest to be identified. In the cases considered, the smallest section of interest was associated with the Jaramillo normal event; digitization intervals and magnetic block widths of about the same size as the measurement interval allowed this smallest section to be identified because it was described by at least two magnetic volume elements.

Equivalent to a discussion of the digitization interval Δy_c is a discussion of the digitization frequency ω_c (radians/km). According to the Theorem of Interpolation (Arsac, 1966), also known as the sampling theorem (Bendat and Piersol, 1966), these two quantities

are related by the expression $\omega_c = \pi/\Delta y_c$. The information content of a field can then be discussed in terms of its frequency content. A quantitative expression of this frequency content is the energy density spectrum $E(\omega)$ (Lee, 1960):

$$E(\omega) = |\Delta t(\omega)|^2$$

where

$$\Delta t(\omega) = \frac{1}{\sqrt{2\pi}} \lim_{L \to \infty} \int_{-L}^{L} \Delta T(y_P) e^{i\omega y_P} \, dy_P$$

is the Fourier transform of the field ($2L$ = magnetic profile length). The energy density spectrum defines the energy content of the field in the frequency band $d\omega$ to be $E(\omega)d\omega$. Therefore, if $E(\omega)$ is known for the measured field, then $\int_0^{\omega_c} E(\omega)d\omega$ will give an indication of the energy content of the field that will be represented by choice of a particular digitization frequency ω_c.

The complete energy density spectrum of the measured field is not known, and it cannot be determined in practice. However, the fields considered here are assumed to be generated by a two-dimensional sequence of source blocks. Therefore, a proportional indication of the measured field energy represented by a particular ω_c can be obtained by determination of the amount of field energy of a single block that is represented by ω_c. The energy density spectrum of the field due to an individual two-dimensional magnetic block

of half-width a and uniform magnetization M, is (Gudmundsson, 1966)

$$E(\omega) = c^2 \frac{\sin^2 \omega a}{\omega^2} \left(e^{-z_1\omega} - e^{-z_2\omega}\right)^2$$

where we find

$$c^2 = 8\pi M^2[(-\cos\tau \sin\psi \cos I \sin\beta' + \sin\tau \sin I)^2 + (\sin\tau \cos I \sin\beta' + \cos\tau \sin\psi \sin I)^2].$$

The angle parameters are shown in Figure 2.

This function is 0 at $\omega = 0$, increases rapidly to a maximum (call $\omega = \omega_m$ at this maximum), and then decreases rapidly to a very small value (call $\omega = \omega_s$ at this small value). For $\omega > \omega_s$ the values of $E(\omega)$ remain very small. Therefore, choice of $\omega_c < \omega_m$ would be a poor representation of the information contained in the field, and choice of ω_c so large that Δy_c is smaller than the measurement interval is unwarranted. We feel that choice of ω_c on the order of ω_s will insure a reasonable representation of the information content of the measured magnetic field.

A test to determine whether a particular block width, and therefore digitization interval, will allow a particular range of field gradients is based on Bernstein's Theorem (Arsac, 1966). This states that the gradient of a function $(\Delta T'(y))$ with a band-limited frequency

content $(0\text{-}\omega_c)$ and maximum amplitude (A) is constrained such that

$$|\Delta T'(y)| \leq \omega_c A$$

For a typical case $\omega_c = 1.5/\text{km}$, $A = 500\ \gamma$, and $|\Delta T'(y)| \leq 1500\ \gamma/\text{km}$. Thus, a wide range of field gradients is possible with these parameters, to the extent that the maximum gradient is much greater than the majority of gradients found in nature.

Application of the Iteration Process to Marine Magnetic Anomalies

Introduction

The importance of marine magnetic anomalies associated with ocean floor spreading has been stressed, and various methods by which the magnetization distributions of source bodies causing these anomalies might be found were presented. In this section the method of iteration is applied to two marine magnetic profiles, one from the South Atlantic Ocean (V20SA, Figures 4, 6, 7) and one of the South Pacific Ocean (EL19N, Figures 5, 6, 7). For each profile the center of each magnetic volume element is chosen to correspond to the position of a digitized field value. This arrangement, together with a digitization interval that allows normal and reverse sections of the source body associated with the shortest paleomagnetic events to be

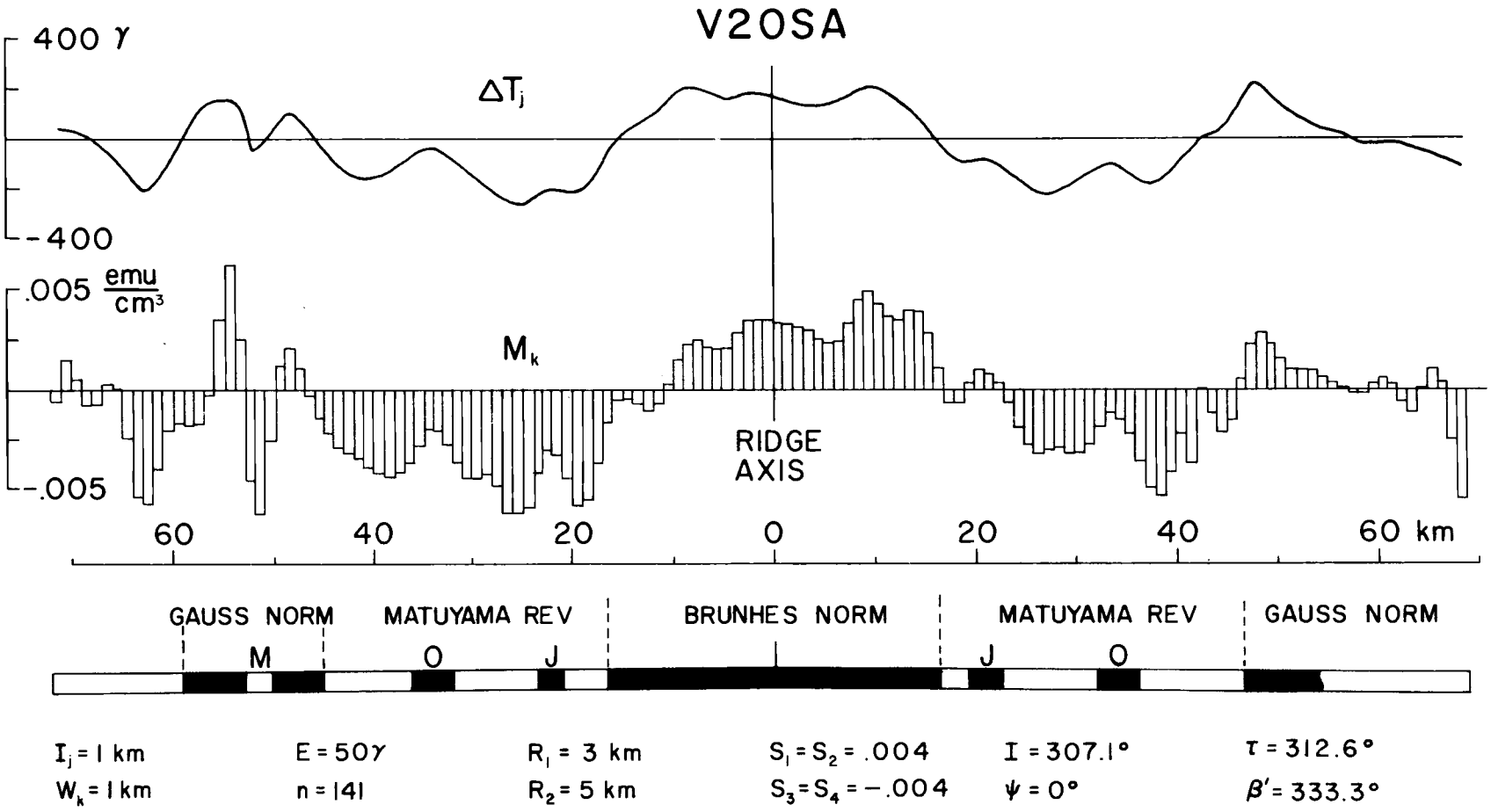

Figure 4. From top to bottom: Digitized version of the V20SA magnetic anomaly profile. Magnetization distribution in the source body. Outline of the source body with sections of normal magnetization (see text) in black; J, O, and M represent the Jaramillo, Olduvai, and Mammoth events respectively. Parameters used in the iteration-process working equations.

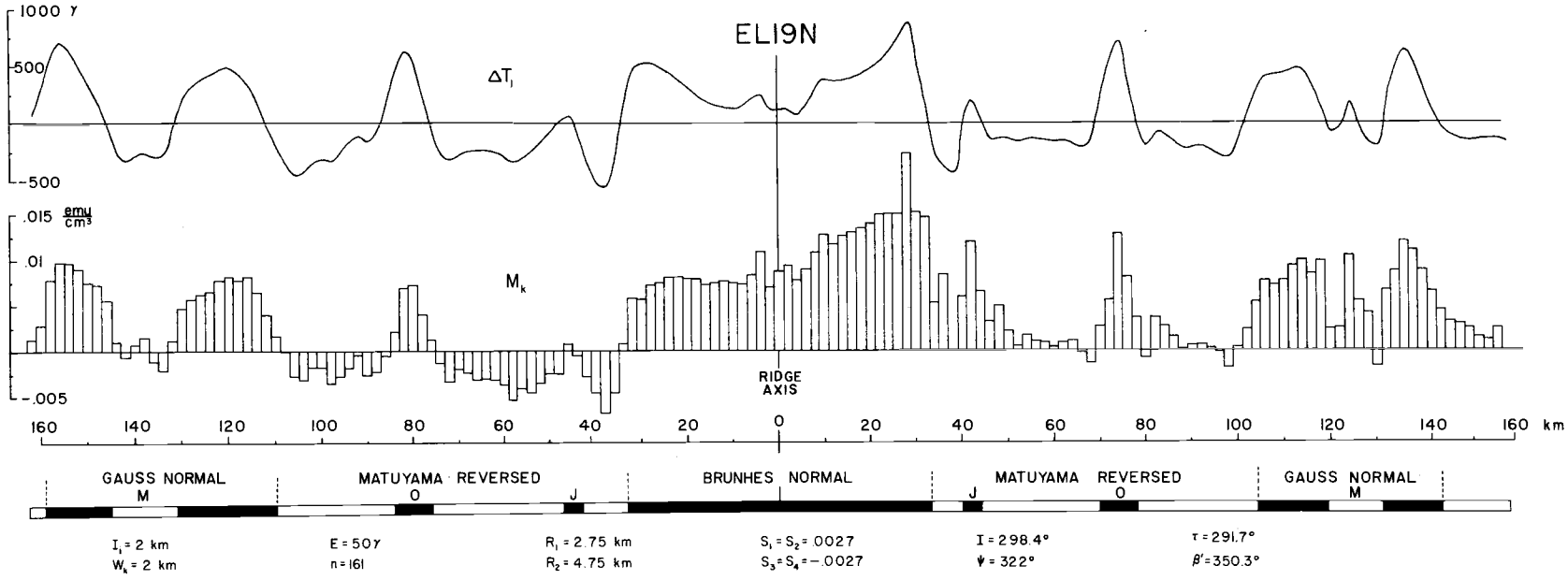

Figure 5. From top to bottom: Digitized version of the EL19N magnetic anomaly profile. Magnetization distribution in the source body. Outline of the source body with sections of normal magnetization in black. Parameters used in the iteration-process working equations.

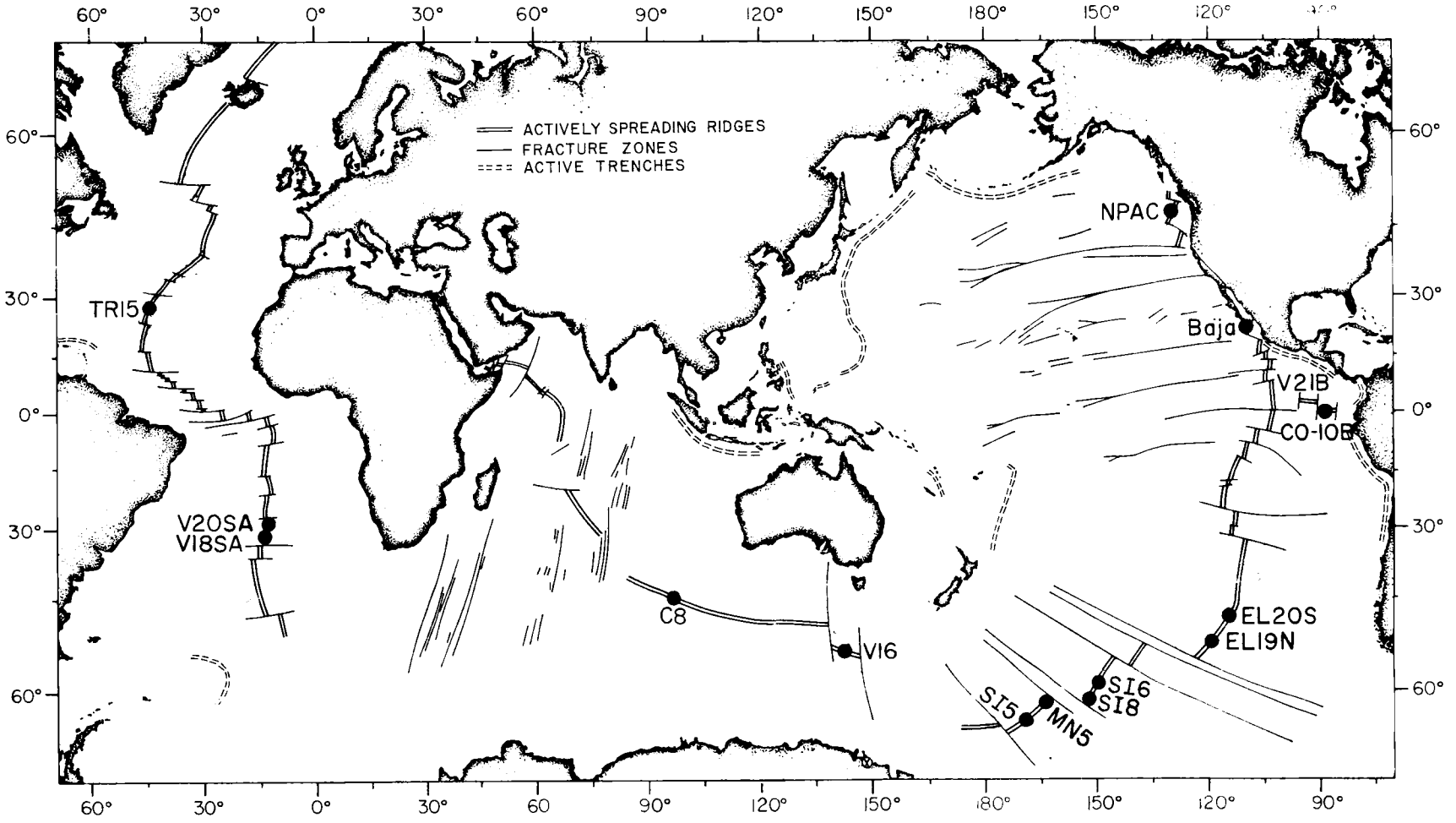

Figure 6. Location of magnetic anomaly profiles for which spreading rate curves are constructed. Adapted from Le Pichon (1968).

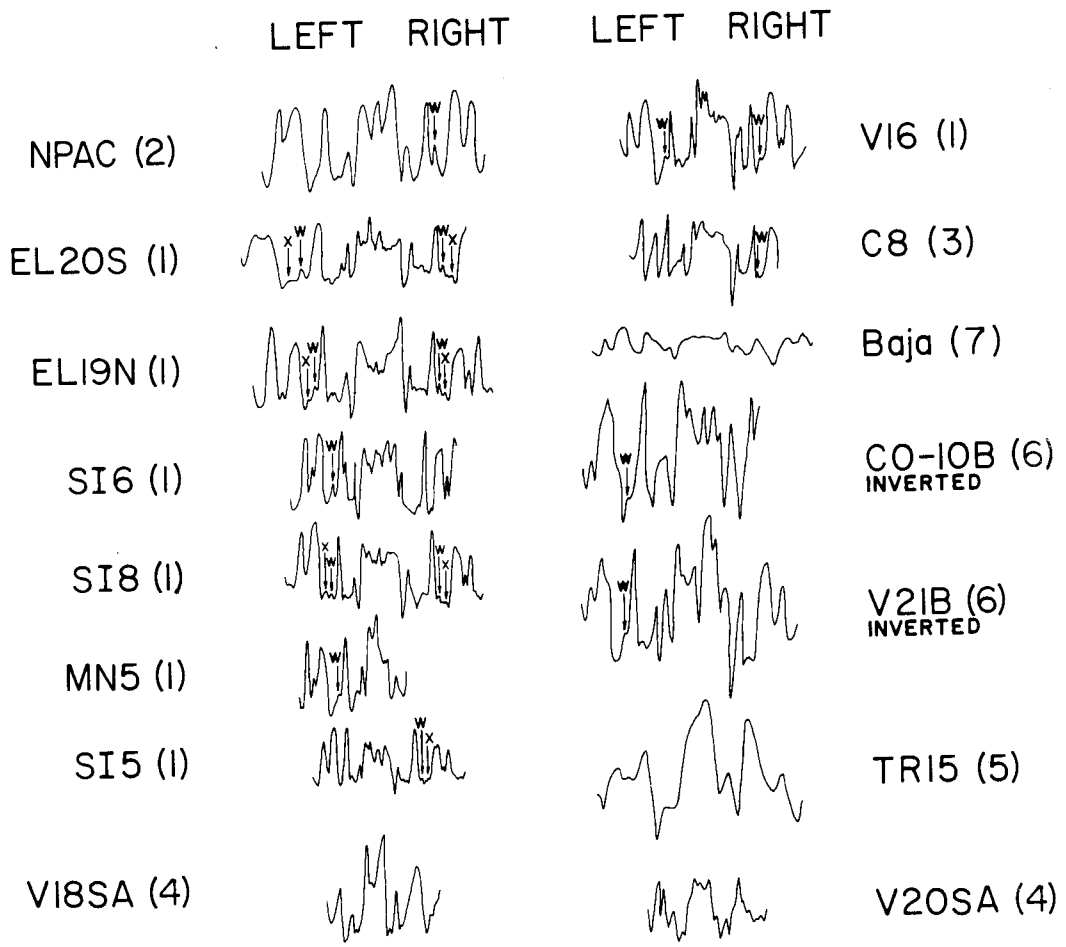

Figure 7. Magnetic anomaly profiles for which spreading rate curves are constructed. Appropriate gamma and kilometer scales are found in the corresponding references: (1) Heirtzler, et al. (1968). (2) Pitman, Herron, Heirtzler (1968). (3) Le Pichon, Heirtzler (1968). (4) Dickson, Pitman, Heirtzler (1968). (5) Phillips (1967). (6) Herron, Heirtzler (1967). (7) Larson, Menard, Smith (1968). The minor anomalies W and X are discussed in the text.

identified, defines the basic physical model to be treated.

The physical stopping norm has been used for the two cases considered here, that is, the iteration process is stopped when the magnitude of the largest component of the residual field vector is less than 50 γ. Since the system is well-conditioned and therefore has a unique solution, the iteration process will always converge. Because the very large number of equations involved for each profile (141 and 161) exceeded the computer storage capacity, each profile was run in three overlapping sections and the solutions given here were obtained by visually comparing and matching results in the regions of overlap. Thus, the regenerated field may differ from the input field by as much as 100 γ in the neighborhood of the points where sections were matched (in regions of low gradient). This is not considered detrimental to the following interpretation.

It is obvious from Figures 4 and 5 that the detail of the magnetization distribution obtained here would be extremely difficult to derive using the indirect method of interpretation. It is also quite evident that the plot of the magnetization values is similar to that of the field values (as the former increase so do the latter).

Moreover, it should be pointed out that negative (positive) field values do not necessarily yield negative (positive) magnetization values. This possible lack of correlation between the algebraic signs of the magnetization values and the field values is due to the dipole

character of the field; it is usually overlooked in applications of the indirect method because of the difficulty involved in incorporating it into the assumptions about the magnetization. Of course, the algebraic sign of the anomaly field depends on the definition of the regional field that was removed from the total field (excellent discussions on the ambiguities of regional field removal are in Grant and West, 1965 and Nettleton, 1954). Also, the relative magnitudes of magnetization values of similar bodies formed at different times depends on the strength of the field at the times of formation. These last two facts require that negative (positive) magnetization values are not necessarily to be identified with reverse (normal) values in the interpretation of a particular magnetization distribution. For this reason, sections of normal and reverse polarity should be chosen by consideration of magnetization contrasts only, with no regard for the algebraic sign of the magnetization values. Sections of normal and reverse polarity resulting from our calculations are shown in Figures 4 and 5.

The Dike Injection Hypothesis

The magnetization distributions presented in Figures 4 and 5 can be interpreted in terms of the ocean floor spreading hypothesis. Dike injection is currently the most widely accepted mechanism (Loncarevic, Mason, and Matthews, 1966; Harrison, 1968) for

bringing mantle material to the surface at the ridge crest. Most of the material causing the magnetic anomalies is believed to have been dike-injected into the crust within a band about 12 km wide. The dike material moves away from the ridge crest as more material is injected to take its place. When geomagnetic field reversals occur, material already in the injection band may become contaminated with oppositely polarized material. A zone of mixed polarities (transition zone between oppositely polarized material) would then be formed which would tend to reduce the effective magnetization of relatively narrow sections of normal or reverse polarity. Dickson, Pitman, and Heirtzler (1968) and Pitman and Heirtzler (1966) have found it necessary to give material under the ridge crest twice the magnetization of the neighboring material in order to approximately reproduce the crestal anomaly. Loncarevic, et al. (1966) suggest that this is physically reasonable because the crestal material which has not yet gone through a field reversal, would not be contaminated by oppositely polarized material and therefore should have a larger effective magnetization. However, the explanation of Loncarevic, et al. (1966) is not acceptable under the hypothesis of a narrow injection band because the contamination zone must also be small, and therefore ineffective in contaminating wide sections of normal and reverse polarity.

In contrast to the indirect-method conclusions of Dickson, et al. (1968) and Pitman and Heirtzler (1966) there is little evidence in

Figures 4 and 5 for abnormally large values of magnetization under the central anomaly, and the crestal section is on the average only slightly more magnetic than its neighboring sections. This result is in agreement with the direct-method findings of Bott (1967), and shows that the neighboring sections are very likely not highly contaminated with oppositely polarized material. This is consistent with the narrow transition zones noted above and in the next paragraph. Slight differences between magnetizations of the older flank material and the relatively new crestal material are to be expected because of the possible decay with time of the older magnetizations (Harrison, 1968).

The magnetization distributions for V20SA and EL19N explicitly demonstrate the narrowness (< 5 km) of the transition zones between sections of normal and reverse polarity. This transition is characterized by gradually changing values of magnetization, but in some cases it could be approximated by a simple discontinuity in the direction of polarization. Therefore, if the dike injection hypothesis of Loncarevic, et al. (1966) and Harrison (1968) is to be accepted, then the dike injection band must in some cases be much narrower than 12 km.

The Paleomagnetic Time Scale

Let us now interpret the magnetization distributions of Figures 4 and 5 in terms of their relation to the experimentally determined

paleomagnetic time scale (Cox and Dalrymple, 1967a). Heirtzler, et al. (1968) demonstrate the world-wide similarity of magnetic profiles across the axial portion of the mid-ocean ridge system; they conclude that each profile may have been generated by the same sequence of two-dimensional source blocks. These authors associate magnetic highs with normally magnetized blocks formed during periods of normal magnetic field, and magnetic lows are associated with reversely magnetized blocks formed during periods of reverse magnetic field. Particular anomalies are named after the events with which they are associated; for example the anomaly usually associated with the Olduvai normal event is called the Olduvai anomaly, and so on. The normal-reverse boundaries (centers of transition zones) of the source bodies in Figures 4 and 5 have been chosen to conform with the model presented by Heirtzler, et al. (1968). This implies that some of the minor normal and reverse sections have not been pictured. Thus, in EL19N the reversed section associated with the Mammoth event is defined (Figure 5) without regard for the suggested normal section within that event (Cox, 1968b). The proposed Gilsa event (Watkins and Goodell, 1967) between the Jaramillo and Olduvai events will be discussed later in relation to the anomaly associated with the Olduvai event.

The normal-reverse boundaries of V20SA and EL19N resulting from the calculations are plotted against the paleomagnetic time scale

in Figure 8. It should be remarked that the distance of each normal-reverse boundary from the ridge axis is known with much more confidence than the corresponding paleomagnetic dates. Therefore, in this analysis the former are assumed to be known exactly, but uncertainties in the latter are considered explicitly. That is, in Figure 8 the ordinate is plotted as a point and the abscissa is plotted as a line segment (the age uncertainty obtained from Cox and Dalrymple, Table 2, 1967b). Straight lines are then drawn between the line segments representing individual magnetic boundaries such that the resulting curves in Figure 8 are as close as possible to straight lines. The slopes of these curves represent the spreading rates for the particular ridge sections.

It is quite evident from Figure 8 that curves representing both left and right sides of V20SA and EL19N are similar; furthermore, the two different profiles result in similar curves. That is, the slopes vary such that the largest slope changes occur with similar characteristics at the Jaramillo and Olduvai events. This is indeed an interesting phenomenon since these profiles are separated by over one thousand kilometers (Figure 6).

In order to investigate the extent of these similarities, spreading-rate curves were constructed for all available profiles where the anomalies usually associated with the paleomagnetic epochs and events could be identified. Locations of these profiles are shown in Figure

6, their axial sections are shown in Figure 7, and the spreading-rate curves are presented in Figures 8, 9 and 10.

Complete magnetization calculations were not made for profiles other than V20SA and EL19N. Figures 4 and 5 indicate that for these profiles the distances of normal and reverse sections of the source body from the ridge axis can be approximated by the distances of their corresponding anomalies from the center of the anomaly over the ridge axis. Therefore, the remaining curves in Figures 8, 9, and 10 were constructed in this approximate manner. The anomalies along a particular profile chosen to represent particular geomagnetic events or epochs are the same as those chosen for that purpose in the original papers (see caption to Figure 7).

The similarity of plots from every profile in Figures 8, 9, and 10 is striking. Only the right side of SI6 (Figure 9) can be fitted by a nearly straight line; all other profiles, including the left side of SI6, have the same characteristic form, even with the large amount of smoothing introduced by consideration of time scale uncertainties. Vine (1966) constructed similar curves for various profiles (without consideration of time scale uncertainties), and fit them with a straight line to determine constant spreading rates since the start of the Gauss epoch. He too noted similar deviations from linearity for two cases, but did not give further discussion. We feel that this phenomenon is important, and that it may have far reaching consequences concerning

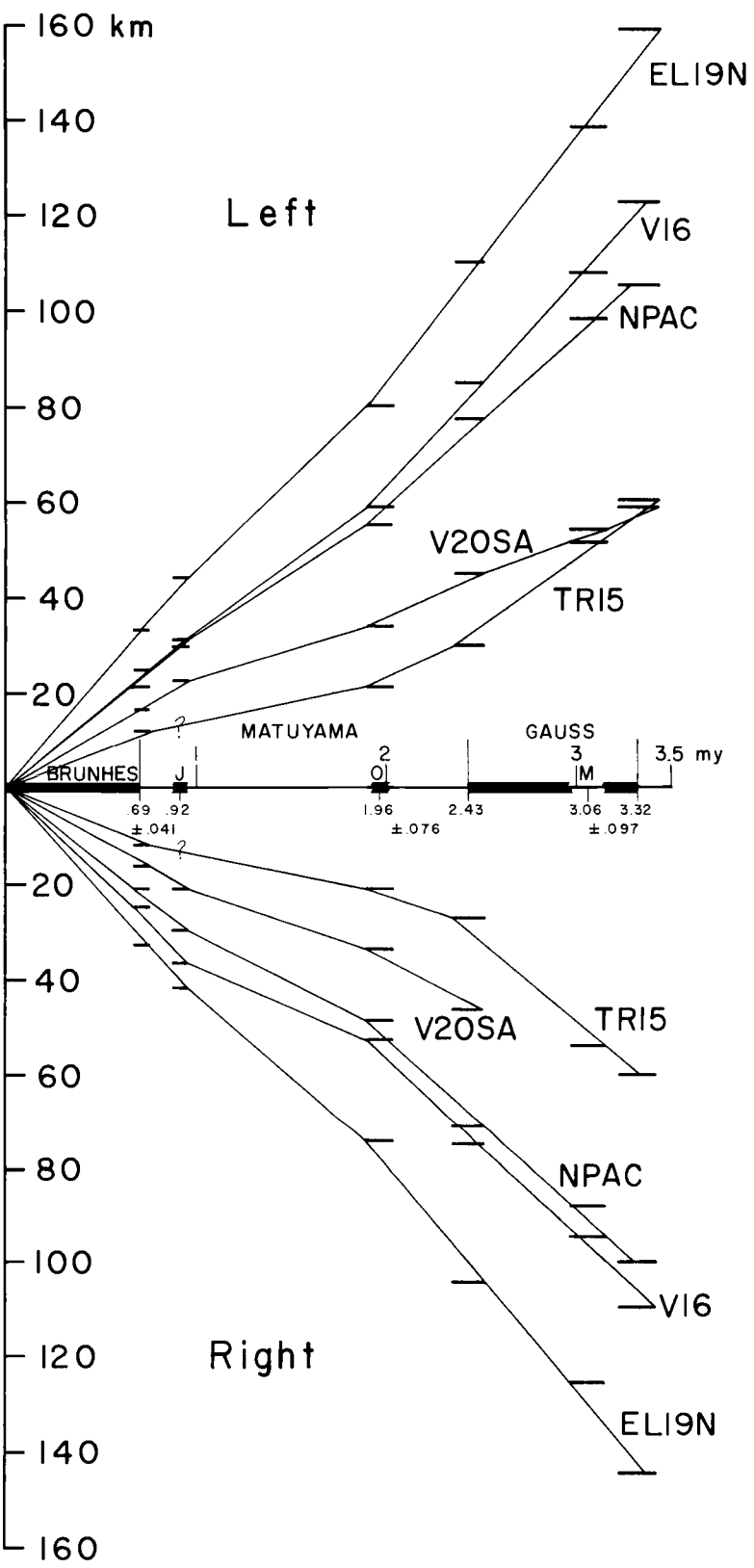

Figure 8. Spreading rate curves. LEFT and RIGHT refer to those sides of the profiles in Figure 7.

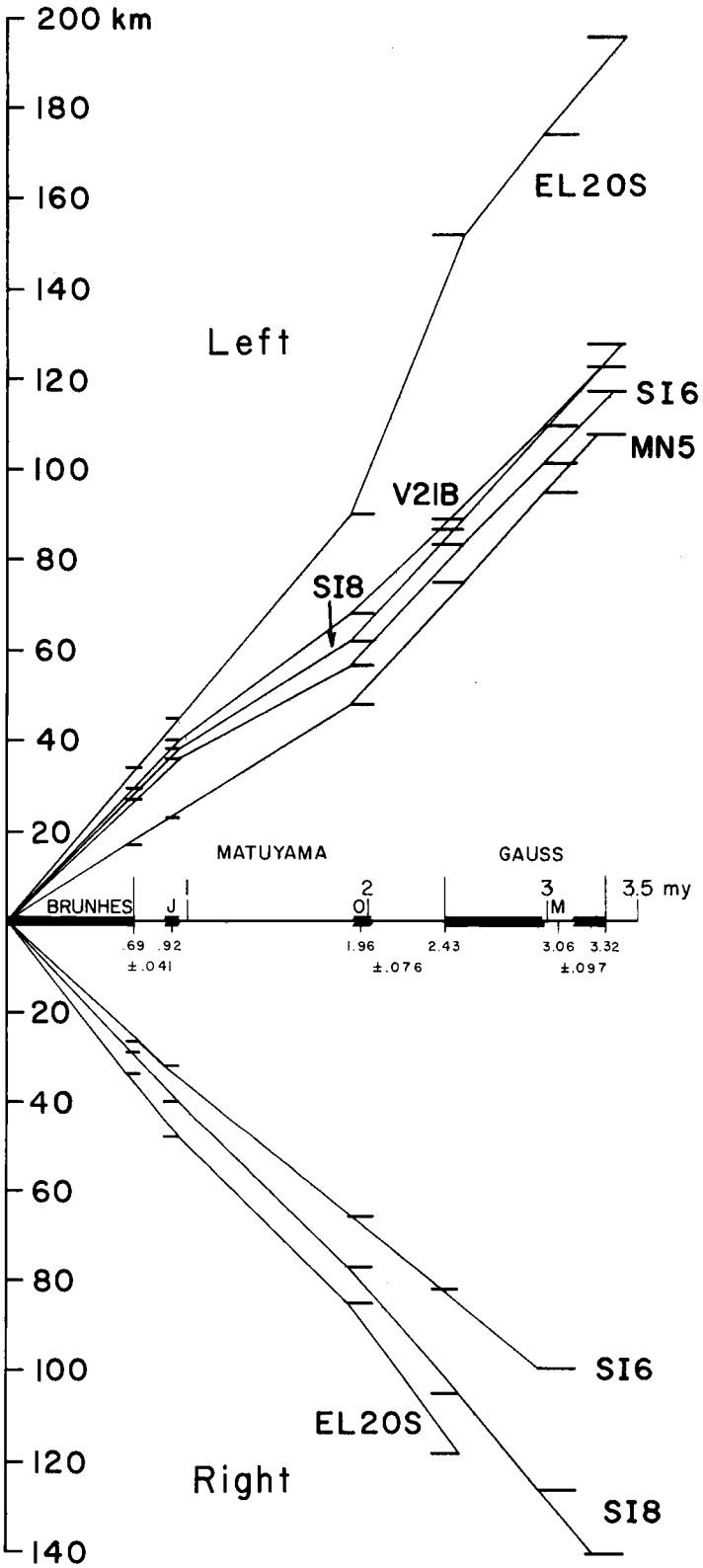

Figure 9. Spreading rate curves. LEFT and RIGHT refer to those sides of the profiles in Figure 7.

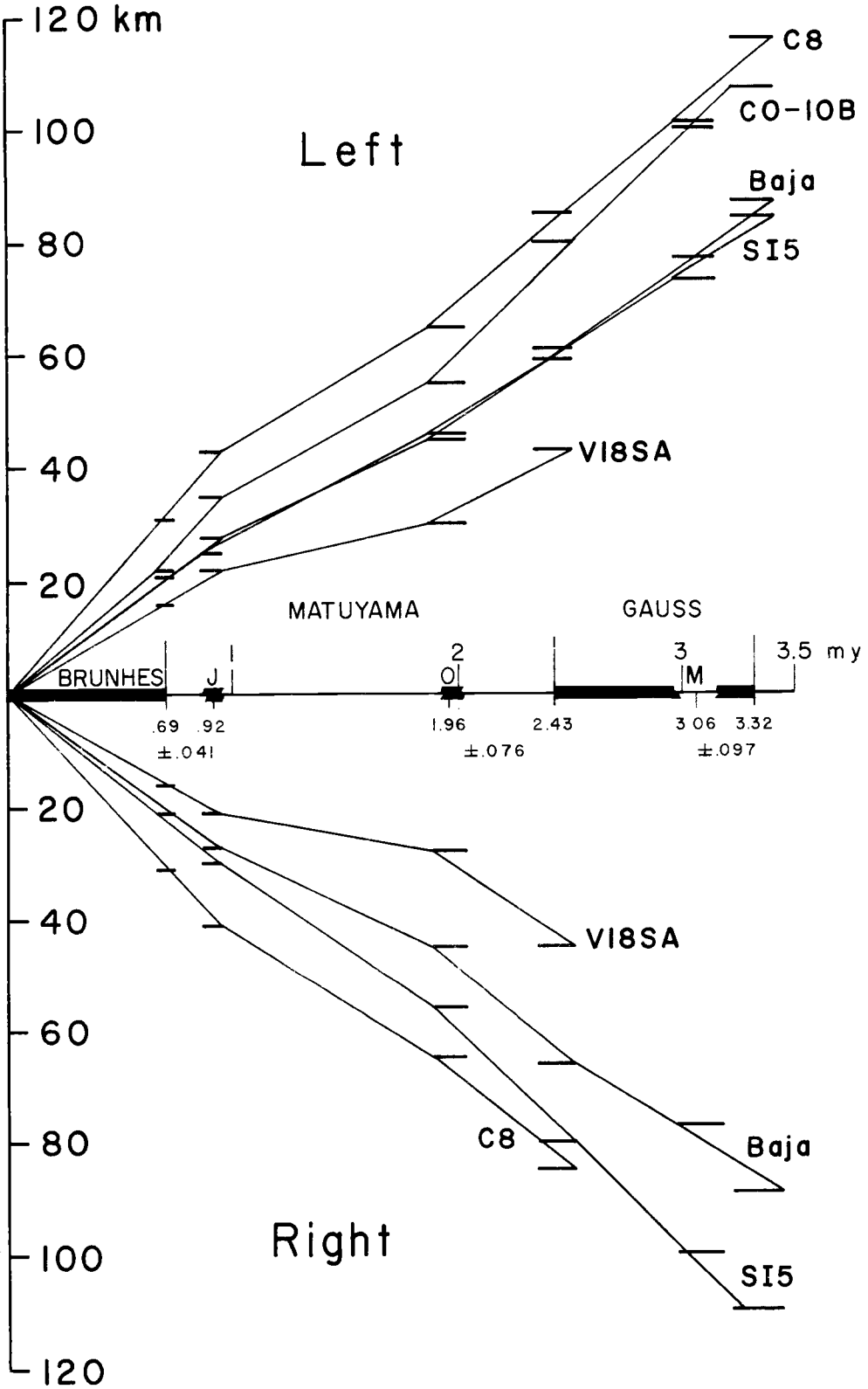

Figure 10. Spreading rate curves. LEFT and RIGHT refer to those sides of the profiles in Figure 7.

mechanisms for ocean floor spreading and/or the validity of accepted relations of certain anomalies to the present paleomagnetic time scale.

Figures 8, 9, and 10 may be interpreted in two ways. First, the postulated relations between the magnetic anomalies and the paleomagnetic time scale are assumed correct and hence, the graphs accurately represent spreading rates of the mid-ocean ridge system for the past 3.32 my (million years). Second, the spreading rates of the ridge system are assumed to have been nearly constant for the past 3.32 my and hence, some of the accepted relations between the anomalies and the paleomagnetic time scale are incorrect.

For the first case, Figures 8, 9, and 10 indicate that spreading rates all along the whole mid-ocean ridge system have changed in the same way, and at the same time during the past 3.32 my. That is, these rates decreased about 2 my before present and then increased at about 0.9 my before present. This would indicate a remarkable world-wide interrelation of movements along the ridge system and would place severe restrictions on any postulates concerning the mechanism for this pattern of movements. Additional evidence of non-uniform movement along the ridge system has recently been reported by Fleischer, et al. (1968). On the basis of radiometric dating of basalt samples they propose the possibility of small, relatively rapid movements for the crestal region of the Mid-Atlantic Ridge at

45° 30' N.

The phenomenon of non-uniform, world-wide movements discussed here would be different than that of episodic spreading, as discussed by Le Pichon (1968) and by Ewing and Ewing (1967), where spreading from mid-ocean ridges is postulated to have stopped completely at various times in geologic history. In this paper the type of spreading indicated by the relatively short time scale, world-wide variation of spreading rates shown in Figures 8, 9, and 10 is referred to as "variable-rate spreading." Le Pichon (1968) proposes that the postulated episodic spreading is strong evidence in favor of the block tectonic theory of ocean floor spreading and against the convection current theory (see the Introduction for a discussion of these theories). He feels that if spreading corresponds to the response of a thick rigid lithosphere to an underlying stress pattern, then all source regions where new material is brought to the surface are interrelated; the dynamic characteristics of these source regions should persist until one or several of the lithosphere blocks become so poorly adjusted to the stress pattern that a readjustment in the world-wide spreading pattern is necessary.

We conclude that if variable-rate spreading exists, it could also be interpreted in favor of the block-tectonic theory. That is, the character of this readjustment of the lithosphere blocks will determine whether episodic or variable-rate spreading takes place. For

example, a system poorly adjusted to the stress pattern may undergo minor readjustments. These minor readjustments would not serve to completely overcome the poor adjustment of the block system to the stress pattern, but would possibly result in the observed variable-rate spreading. On the other hand, if a system undergoes a major readjustment, then eposodic spreading could result.

Let us now take the second approach to the interpretation of Figures 8, 9, and 10, and investigate the possibility that the spreading rates have been more or less constant for the past 3.32 my. This would imply errors in the postulated relations between the magnetic anomalies and the paleomagnetic time scale, although it is well known that some of the relations are regarded as highly reliable (for example, the start of the Brunhes and Gauss epochs). The interpretation of Figures 8, 9, and 10 should therefore be in accord with the most reliable relations between the anomalies and the time scale.

Constant, or nearly constant, spreading can be represented in three ways: (1) by a least-square (fixed-origin) straight line fit of the curves (a straight line fit was used by Vine (1966) but he did not mention if a least-square criterion was used.) (2) By a straight line extrapolation of the straight line connecting the origin and the start of the Brunhes epoch; that is the timing interval representing the start of the Brunhes is assumed to be fixed. (3) By a broken line (fixed origin) drawn under the assumption that the timing intervals

representing the start of the Brunhes, the center of the Jaramillo, and the start of the Gauss are fixed. It is shown below that (3) is the most likely way of accounting for nearly constant spreading for the past 3. 32 my.

If constant spreading is assumed and represented for all graphs by a least-square fit as described in (1) then many of the plotted intervals for the timing of paleomagnetic events would deviate from (that is, would not intersect) the least-square lines. As these lines are required to be accurate indications of spreading rates for the past 3. 32 my, it must be concluded that the paleomagnetic time scale is incorrect for all time intervals deviating from them. These deviations are inconsistent from one graph to another, thus indicating that the time scale is correct for some profiles and not others, that is, it is correct in some parts of the ridge system and not in others. This result cannot be accepted because of evidence for simultaneous worldwide occurrence of paleomagnetic epochs and events.

The assumption made in adopting procedure (2) to represent constant spreading for the past 3. 32 my is quite reasonable. That is, the start of the Brunhes epoch has been dated with a high degree of confidence, and it is readily associated with the central magnetic anomaly. However, many of the plotted time intervals do not consistently intersect the resulting straight lines and the objections raised to the validity of procedure (1) can also be applied here.

Procedures (1) and (2) will, therefore, not be considered further.

The plot of the timing interval representing the start of the Gauss epoch is known with some confidence, and the assumptions necessary for application of procedure (3) are therefore acceptable. Examination of Figures 8, 9, and 10 shows that application of procedure (3) is equivalent to constant spreading rates from 3. 32 to 0. 9 my followed by changes in the spreading rates. These changes are such that for some profiles the spreading rate increased slightly, and for other profiles it decreased slightly at about 0. 9 my. In Figure 11 profile EL19N is used as an example of application of procedure (3). Unlike the undesirable situation encountered from applications of procedures (1) and (2), where many plotted timing intervals did not consistently intersect the resulting lines, only one timing interval consistently does not intersect the lines from application of procedure (3). This interval represents the Olduvai event and it always lies on the positive time-axis side of the line representing constant spreading from 3. 32-0. 9 my. The implication would be that under the hypothesis of constant spreading from 3. 32-0. 9 my the anomaly usually associated with the Olduvai event should be associated with some younger normal event. The approximate age of such an event can be derived from the curves in Figures 8, 9, and 10. All curves except TR15 are considered in the derivation; this curve is not considered because it is the only one where a timing interval, other than the

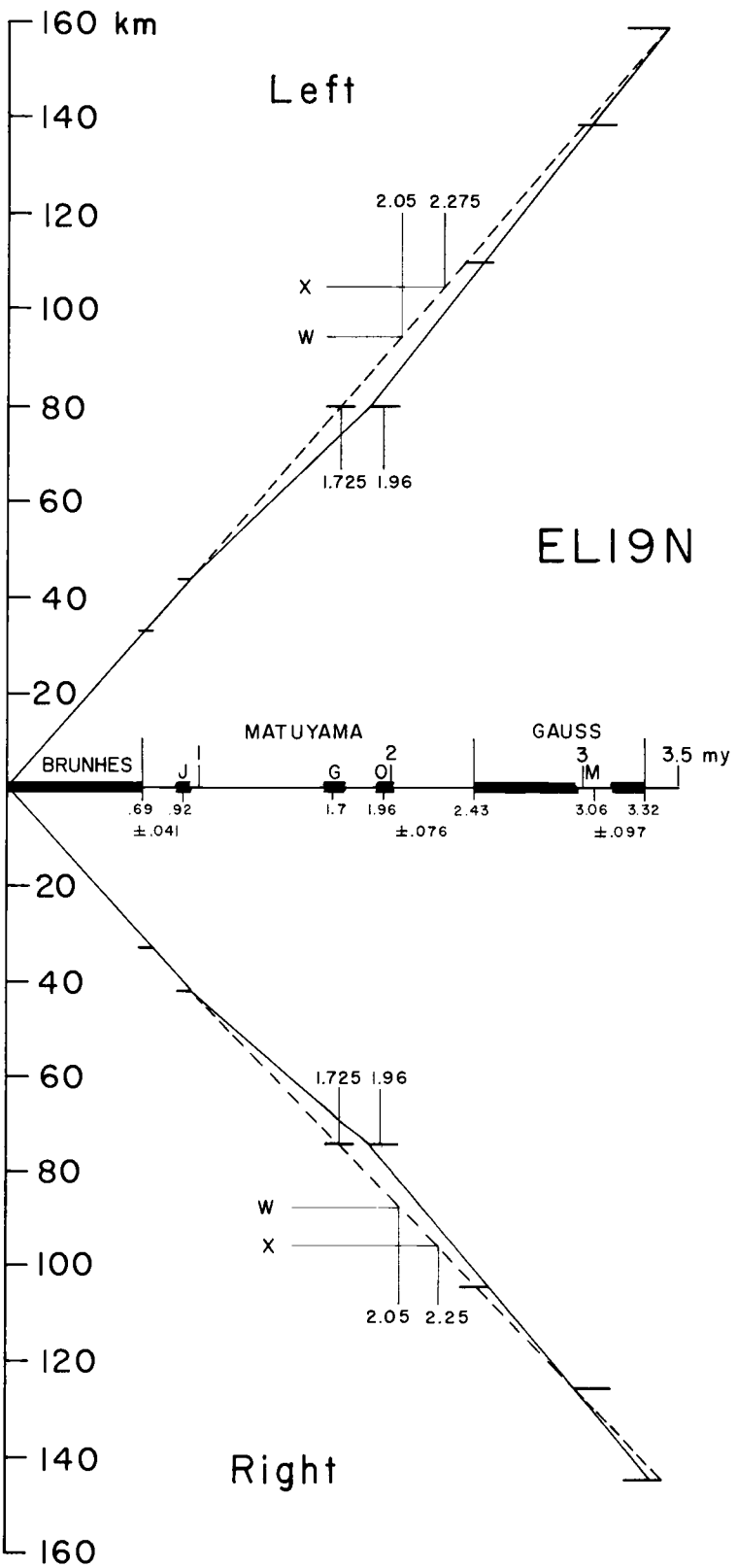

Figure 11. Application of procedure (3) (see text) to EL19N. G represents the Gilsa normal event.

"Olduvai interval, " does not intersect the line representing constant spreading from 3. 32 to 0. 9 my. Therefore, if procedure (3) is carried out for all profiles except TR15, and if the center of the "Olduvai interval, " originally at 1. 96 my, is required to lie on the resulting line, then the average age of this younger normal event should be about 1. 66 my (s. d. = 0. 88 my). This derivation is shown explicitly in Figure 11 for EL19N where the age of the younger event turns out to be 1. 725 my.

A younger normal event, the Gilsa event, shown in Figure 11, exists (McDougall and Wensink, 1966; Watkins and Goodell, 1967; Cox and Dalrymple, 1967a) and is dated at about 1. 7 my (A. Cox, personal communication, 1968a). No particular magnetic anomaly has been associated with the Gilsa event because no obvious anomaly consistently appears between the ones usually associated with the Olduvai event (1. 96 my) and the Jaramillo event (0. 92 my). Application of procedure (3) therefore implies that the Gilsa anomaly, till now undefined, may be the anomaly usually associated with the Olduvai event. Similar ideas have been expressed by A. Cox (personal communication, 1968a).

There is extensive evidence for the existence of the Olduvai normal event at 1. 96 my and it is reasonable to expect an anomaly associated with this event. That is, if the anomaly usually associated with the Olduvai event is associated with the Gilsa event, then there

should be some other consistently appearing anomaly which may be associated with the Olduvai event.

Heirtzler et al. (1968) discuss a minor anomaly, called X, which occurs with some consistency between the anomalies associated with the Olduvai event and the end of the Gauss epoch. This anomaly X and a neighboring anomaly W which also consistently appears, are labeled in Figure 5. Anomalies X and W sometimes occur as a doublet and sometimes only one or the other appears. In the latter case it cannot be determined by simple examination of the profiles which anomaly is present. In order to overcome this difficulty the age of each pertinent anomaly was determined for all the profiles from the assumed constant spreading rates from 3.32 to 0.9 my. Using only the profiles containing both anomalies the average age of W turns out to be 2 my (s.d. = 0.06 my) and the average age of X is 2.3 my (s.d. = 0.1 my). The ages for X and W in EL19N are shown explicitly in Figure 11. When a single anomaly occurred it was subsequently labeled W or X depending on its relation to the previously determined average ages for W and X. All singly appearing anomalies corresponded to W, and no ambiguities were encountered. The resulting average age of W (1.99 my) corresponds very closely to the measured age of the Olduvai event (1.96 my) and we postulate that under the assumption of constant spreading from 3.32 to 0.9 my, W is the true Olduvai anomaly.

The question now arises as to which of the two interpretations of Figures 8, 9, and 10, variable rate spreading or case (3) of nearly constant spreading, is more acceptable. If the variable-rate spreading interpretation is accepted then there is no anomaly that can be easily related to the Gilsa event. If a constant spreading rate from 3.32 to 0.9 my is accepted then both the Gilsa and the Olduvai events can be associated with consistently appearing anomalies. We tend to regard the latter case as more acceptable than the former because of the quite natural way it allows all the well known paleomagnetic events to be associated with consistently appearing magnetic anomalies.

The constant spreading interpretation gives support to the assumption of many authors that the ocean floor has been spreading at a nearly constant rate for the past 10 my. For example, if the usual Olduvai event-anomaly association, and therefore the variable-rate spreading hypothesis, is accepted, then obviously the assumption of constant spreading over this period becomes quite tenuous. This evidence tending to support the assumption of constant spreading for the past 10 my is, however, somewhat weakened by the evidence for slight spreading changes around 0.9 my.

THE OVERDETERMINED PROBLEM

Introduction

In the previous discussion on methods of solution of the direct problem, the number of magnetic volume elements was taken to be equal to the number of field input points. This allows us to obtain a unique solution to a well-conditioned problem involving an assumed model geometry. In other words, there is exact agreement at the input points between the observed field and the field generated by the solution distribution. However, the two fields will deviate in the intervals between these points. For a given number of field points the present method does not provide a means of estimating the magnitude of this deviation.

There now appear to be two options for improving the overall agreement between the observed and the computed fields. First, the number of input points (m) and the number of magnetic volume elements (n) can be increased, still keeping $n = m$. This will result in an exact agreement of the observed and the computed fields at a greater number of field points, at the expense of a greater computational effort. Second, in the case of a given number of magnetic volume elements, the number of input points can be increased. An exact agreement can no longer be attained at the input points. This procedure therefore requires the minimization of some norm-function

of the deviations between the observed and the computed fields at the input points. This leads to an overdetermined problem in computing the magnetization distribution.

Moreover, once a solution has been obtained for the well-conditioned problem with $n = m$, it is often desirable to test the sufficiency of simpler physical models; that is, models with a smaller number of magnetic volume elements but where the number of input points is unchanged. This third case, involving $n < m$, will naturally lead to the same type of computational problem as the second option above. That is, to an overdetermined problem where some norm-function of the deviations is to be minimized.

In discussing the merits of these three variations to the direct problem, it is to be realized that imposition of an exact agreement between the observed and computed fields at a given number of input points is an unwarranted accuracy. All input data contain measurement and data reduction errors and, furthermore, the above procedure is based on an assumed model geometry which will deviate from the real geometry of the magnetized material.

No further discussion is necessary in the case of the first option involving $n = m$. On the other hand, the two latter cases lead to a different kind of computational problem which will be discussed here. For practical reasons, the discussion of the overdetermined problem will be based on the third case where the number of input points is

fixed.

In order to state the practical overdetermined problem in its full generality a further physical constraint should be taken into account. The possible values of the magnetization are bounded from above, and a direct sampling of the magnetization of natural rocks in a particular region (see for example Tarling, 1966) may supply an upper limit to the acceptable values of M_k.

Formal Statement of the Overdetermined Problem

Introducing the slack variables s_j, the general problem of determining the M_k can be stated in the following way:

$$\Delta T_j = \sum_{k=1}^{n} G_{jk} M_k + s_j \quad (j=1, \ldots, n) \tag{15}$$

$$f(s_j) = \min,$$

$$|M_k| < M_{max}.$$

This is, given the m field values ΔT_j, determine the n values M_k such that some suitable norm-function $f(s_j)$ of the differences between ΔT_j and $\sum_{k=1}^{n} G_{jk} M_k$ is minimum. The M_k thus obtained are then taken as estimates (in the sense of the norm-function used) of the magnetization distribution.

The most important and frequently used norm-functions (norms)

are members of the class of L_p norms (Rice, 1964) defined as follows:

$$f(s_j) = L_p(s_j) = \left[\sum_{j=1}^{m} |s_j|^p \right]^{1/p} = \min$$

with $L_p(s_j) \geq 0$, and $L_p(s_j) = 0$ if and only if $s_j = 0$. Rice and White (1964) discuss the criteria for choosing different values of p; in particular, they compare results for the L_1, L_2, and L_∞ norms for a given example. These are the three norms considered in this paper. In a more familiar representation they are

(16) $p = 1$, $\sum_{j=1}^{m} |s_j| = \min$;

$p = 2$ (least squares), $\sum_{j=1}^{m} (s_j)^2 = \min$;

$p = \infty$ (minimax or Tchebycheff), $\max_j |s_j| = \min$.

Rice and White (1964) conclude that for approximation purposes the L_1 norm is best suited to situations where large residual values (the error at a particular point) are not uncommon; that is, the statistical distribution of the residuals has a long tail which allows "wild points." On the other hand, the L_∞ norm is best suited to systems

where the residual distribution has sharply defined limits and the L_2 norm is best suited to residual distributions lying between these extremes.

We must now ask what assumptions or characteristics of the problem under consideration here will affect the values of the slack variables s_j. Essentially, a model $(\sum_{k=1}^{n} G_{jk}M_k)$ is being fitted to reality ΔT_j. Model disparity (the difference between model and reality) in well-conditioned problems can result in both a physical and a numerical way; the former results from the choice of a basic model that is not truly representative of the source body causing the anomaly field, and the latter results when the number of unknowns (n) differs from the number of field points (m). Numerical model disparity is a direct function of the difference between m and n and is absent when m = n; physical model disparity is unavoidable because of the very nature of geophysical interpretation. Of course, when m = n and the system is well-conditioned any effect of physical model disparity is masked because the system then has a unique mathematical solution.

The character of the deviations between the observed field and the field calculated on the basis of the M_k solutions obtained from Equation (15) using L_p type norms will depend on the index number p. The distribution of the magnitude of the deviations at individual points will become increasingly uniform with increasing p. The

L_1 norm will give a relatively heterogeneous distribution with possibly a number of large deviations, whereas the L_∞ norm will give a very uniform distribution.

In choosing the most suitable norm the computational effort has to be taken into consideration. In this respect the L_2 norm is superior.

The effects of the three norms L_1, L_2, and L_∞ will be displayed below through the use of examples.

Methods of Treatment of the Overdetermined Problem

Methods of treatment of Equation (15) using the above norms will now be presented. The L_1 and L_∞ norms will be treated first, and then the L_2 norm will be treated in both an exact and an approximate manner. No constraint on the magnitude of M_k will be considered explicitly.

The most readily available method of estimating the magnetization distribution from Equation (15) using the L_1 and L_∞ norms of Equation (16) is that of linear programming (LP). A brief outline of the LP method along with pertinent theorems and definitions is given in the Appendix.

The L_1 Norm

The variables of the LP primal problem are required to be

non-negative. The variables M_k and s_j are not necessarily non-negative, but they can be expressed in terms of other variables which are always non-negative. The slack s_j is written as the difference between two non-negative slacks (u_j, v_j); according to Equations (4) in the Appendix, M_k can be written

$$M_k = N_k - C, \quad N_k \geq 0, \quad C = \text{const.}$$

The first of Equations (15) then takes the form

$$\sum_{k=1}^{n} G_{jk} N_k + u_j - v_j = T_j \tag{17}$$

where

$$T_j = \Delta T_j + C \sum_{k=1}^{n} G_{jk},$$

$$N_k \geq 0, \quad u_j \geq 0, \quad v_j \geq 0.$$

These equations are identical in form to the constraints and non-negativity conditions of the standard LP problem. The L_1 norm defines the objective function; that is (Equation (16))

$$L_1(s_j) = \sum_{j=1}^{m} |u_j - v_j| = \sum_{j=1}^{m} (u_j + v_j) = \min$$

since for each value of j only one of the slack variables can be

non-zero. The standard LP formulation (see Equations (1), (2), (3), in the Appendix) for the L_1 norm is then

$$(18) \qquad \sum_{k=1}^{n} G_{jk}N_k + u_j - v_j = T_j \quad (j=1, \ldots, m),$$

$$N_k \geq 0, \quad u_j \geq 0, \quad v_j \geq 0,$$

$$\sum_{j=1}^{m} (u_j + v_j) = \min$$

where

$$M_k = N_k - C, \quad C = \text{const},$$

$$T_j = \Delta T_j + C \sum_{k=1}^{n} G_{jk}.$$

It is mentioned in the Appendix that an upper bound ($|M_k| \leq M_{max}$) on the magnitude of N_k, and therefore M_k, can be explicitly incorporated into the LP formulation. The constraint expressing this upper bound

$$-C \leq N_k \leq M_{max} - C$$

will not be considered further.

The dual LP formulation will shorten the computations when $m > n$. The dual is obtained by first expressing the primal problem

as follows:

$$\sum_{k=1}^{n} G_{jk} M_k + u_j - v_j = \Delta T_j \quad (j=1, \ldots, m),$$

$$M_k \quad \text{unrestricted in sign,}$$

$$u_j \geq 0, \quad v_j \geq 0,$$

$$\sum_{j=1}^{n} (u_j + v_j) = \min.$$

According to the rules presented in the Appendix the dual problem is then

$$\sum_{j=1}^{m} G_{jk} x_j = 0 \quad (k=1, \ldots, n),$$

$$-1 \leq x_j \leq 1,$$

$$\sum_{j=1}^{m} \Delta T_j x_j = \max.$$

To express this in terms of non-negative variables let $x_j = y_j - 1$. Then the reduced dual formulation for the L_1 problem is

$$(19) \qquad \sum_{j=1}^{m} G_{jk} y_j = \sum_{j=1}^{m} G_{jk} \quad (k=1, \ldots, n),$$

$$0 \leq y_j \leq 2,$$

$$\sum_{j=1}^{m} \Delta T_j y_j = \max$$

where the constant term $-\sum_{j=1}^{m} \Delta T_j$ has been deleted from the objective function because it adds nothing to the problem.

The L_∞ Norm

Application of the L_∞ norm involves the minimization of the maximum component of the residual vector. That is, from Equation (16)

$$L_\infty(s_j) = \max_j |s_j| = \max_j \left| \Delta T_j - \sum_{k=1}^{n} G_{jk} M_k \right| = \min \quad (j=1, \ldots, m).$$

If the unknown maximum value is represented by the new variable E, then the L_∞ norm can be represented as

$$\left| \Delta T_j - \sum_{k=1}^{n} G_{jk} M_k \right| \leq E,$$

$$E = \min.$$

Upon removal of the absolute value sign and rearrangement, this expression becomes

$$E + \sum_{k=1}^{n} G_{jk} M_k \geq \Delta T_j \quad (j=1, \ldots, m),$$

$$E - \sum_{k=1}^{n} G_{jk} M_k \geq -\Delta T_j,$$

$$E = \min.$$

If we neglect for the moment that M_k is unconstrained in sign, then these equations are the constraints and objective function of the LP problem. But, in comparison with the L_1 primal formulation (Equations (18)) there are here twice as many constraints (2m), and hence the computation time is increased considerably. To eliminate this unwanted condition we express the above L_∞ equations in their dual form with the help of Theorem (c) in the Appendix:

$$(20) \qquad \sum_{j=1}^{m} G_{jk} y_j - \sum_{j=m+1}^{2m} G_{j-m,\,k} y_j = 0 \quad (k=1, \ldots, n),$$

$$\sum_{j=1}^{2m} y_j = 1,$$

$$\sum_{j=1}^{m} \Delta T_j y_j - \sum_{j=m+1}^{2m} \Delta T_{j-m} y_j = \max.$$

Equations (19) and (20) constitute the formal basis for estimation of the magnetization distribution using the L_1 and L_∞ norms.

The L_2 Norm

Discussion of the L_2 norm has been saved till last because it turns out to be the norm best suited to the problem considered in this paper, from both a computational and a physical standpoint.

Tanner (1967) gives the following formal procedure for expressing Equation (15) in a form suitable for treatment using the L_2 norm when $m \geq n$: Determination of M_k from

$$\Delta T_j \simeq \sum_{k=1}^{n} G_{jk} M_k \qquad (j=1, \ldots, m \geq n),$$

subject to the condition

$$L_2(s_j) = \sum_{j=1}^{m} (\Delta T_j - \sum_{k=1}^{n} G_{jk} M_k)^2 = \min,$$

requires that

$$\frac{\partial L_2(s_j)}{\partial M_r} = -2 \sum_{j=1}^{m} G_{jr} (\Delta T_j - \sum_{k=1}^{n} G_{jk} M_k) = 0 \qquad (r=1, \ldots, n)$$

or, equivalently

$$\sum_{j=1}^{m} G_{jr} \Delta T_j = \sum_{j=1}^{m} \sum_{k=1}^{n} G_{jr} G_{jk} M_k \qquad (r=1, \ldots, n). \tag{21}$$

Equation (21) is a system of n equations in n unknowns. In

matrix notation it is

$$G^T \Delta\vec{T} = G^T G\vec{M}$$

where G^T represents the transpose of G. At this point it should be noted that when no restrictions are placed on the relation between m and n the L_2 norm can be treated using the method of quadratic programming (Hadley, 1964), but this is not considered further.

Determination of the magnetization distribution using the L_2 norm then reduces to the problem of solving an $n \times n$ system of linear equations. Methods of doing this were discussed earlier where only the $n = m$ case was considered. In that discussion it was pointed out that the method of iteration makes it possible to explicitly consider the sufficiency of a magnetic model. Through solution of the overdetermined problem the physical model sufficiency can be explicitly considered. Therefore, if the method of iteration is used to solve Equation (21) then magnetic model sufficiency can be considered in conjunction with physical model sufficiency. This cannot be done when either the L_1 norm or the L_∞ norm is used to treat the overdetermined problem. Difficulties do arise, however, when both magnetic and physical sufficiency are considered. That is, there is no unique solution and the possibility of the iteration process reaching a physical and not a mathematical termination is surely diminished.

From a computational point of view the determination of the

magnetization distribution using the L_2 norm, through Gaussian reduction or iteration, is much simpler and less expensive in terms of computer time than if the L_1 norm or the L_∞ norm is used. However, as the LP system at Oregon State improves it will become much more versatile and easier to use (L. Scheurman, personal communication, 1968). It will then be possible to take better advantage of its special properties when using the L_1 and L_∞ norms.

Application of Exact Methods and a Comparison of Results Using the L_1, L_2, and L_∞ Norms

As an aid to understanding the behavior of all three norms, let us now use them to interpret one magnetic anomaly profile in terms of three different physical models.

Figure 12 shows a digitized version of the central segment of Profile 40 from the Reykjanes Ridge (Heirtzler, Le Pichon, and Baron, 1966), the three physical models to be considered, and the parameters to be used in the working equations. Differences in the models lie solely in the number and widths of their component blocks. The same field input points are used for each model. It is obvious from this figure that the $n = 17$ model will be significantly poorer than the $n = 25$ model, which in turn will be significantly poorer than the $n = 37$ model.

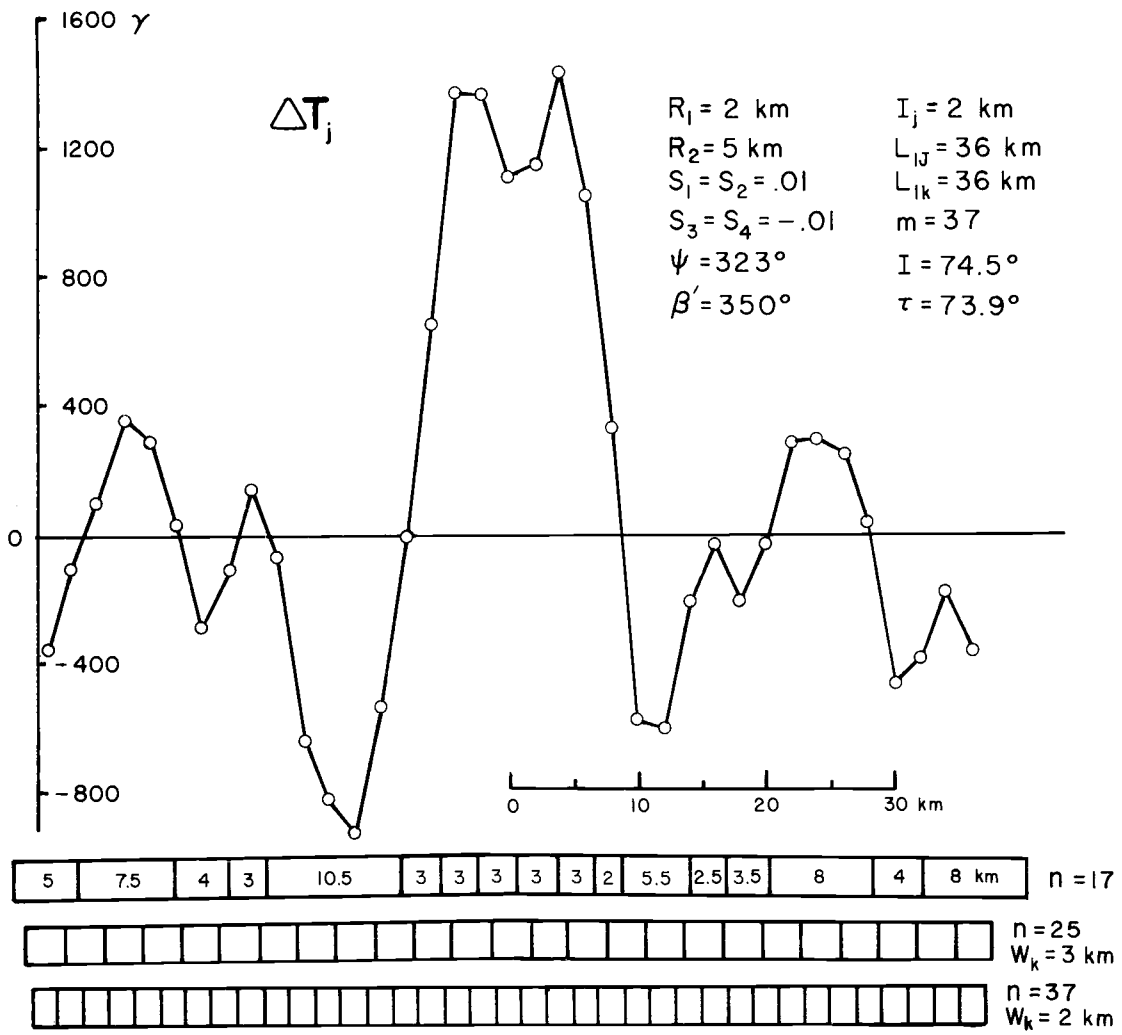

Figure 12. Crestal region of the Reykjanes Ridge. Digitized input field, parameters used in the working equations, and the models used to fit the input field. No vertical exaggeration on the 3 km thick models.

Figure 13 shows the magnetization distribution for the $n = 37$ model which, of course, generates the input field exactly. For the $n = 25$ model Figures 14, 15, and 16 show the L_1, L_2 and L_∞ magnetizations respectively along with their residual fields. The residual field is defined as the input anomaly field minus the field recalculated from the particular magnetization distribution. Figures 17, 18, and 19 show the same quantities for the $n = 17$ model. No requirement on the maximum value of M_k was incorporated into these calculations.

It is evident from Figures 14 through 19 that for each model a choice of a suitable norm reduces to a decision on what behavior is desired for a residual field. As expected, the L_1 norm gives a residual field with many small values and some very large values, the L_∞ norm gives a residual field with many intermediate values, and the L_2 norm gives a field between these extremes. However, when the positions of large residual field values are compared to the position of the pertinent input points (Figure 12) an interesting relationship becomes apparent; the largest residual field values of the L_1 and L_2 norms correspond to regions of very high gradient in the input field, while the largest values for the L_∞ norm are spread throughout the input profile. In many applications of the magnetic interpretation method the largest interpretation errors are to be expected and accepted in regions of high gradient, because of the

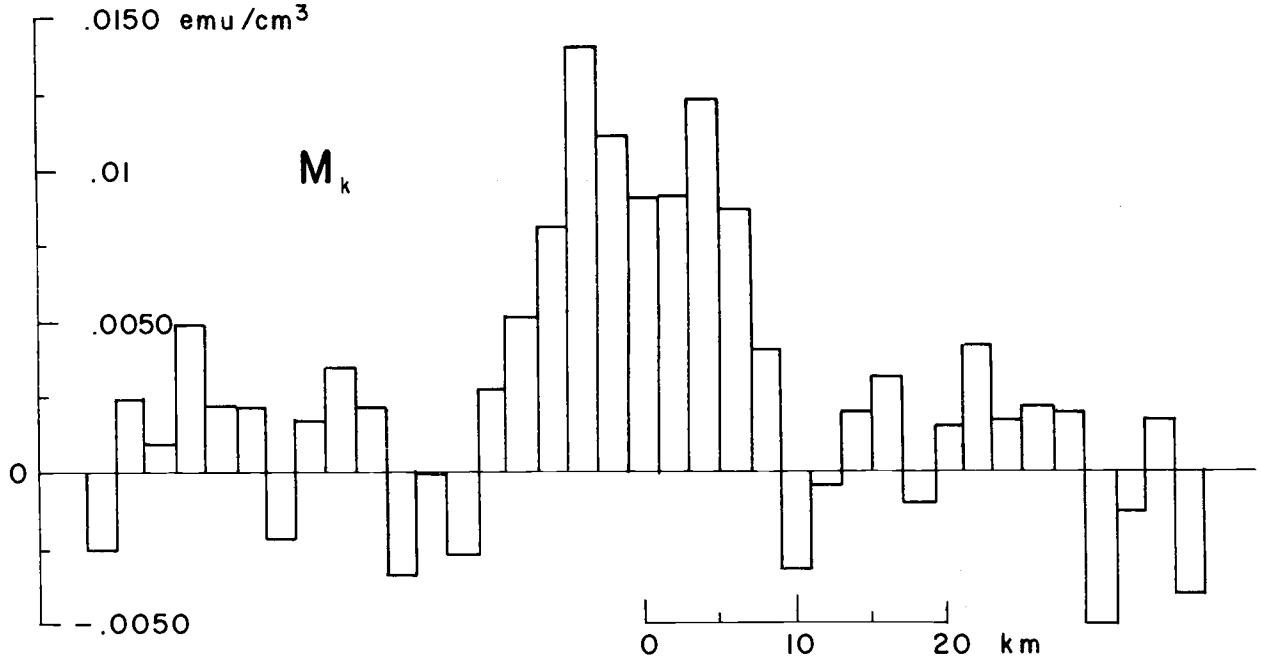

Figure 13. Magnetization values for the n = 37 model. These values generate the input field exactly, and the residual field values are zero.

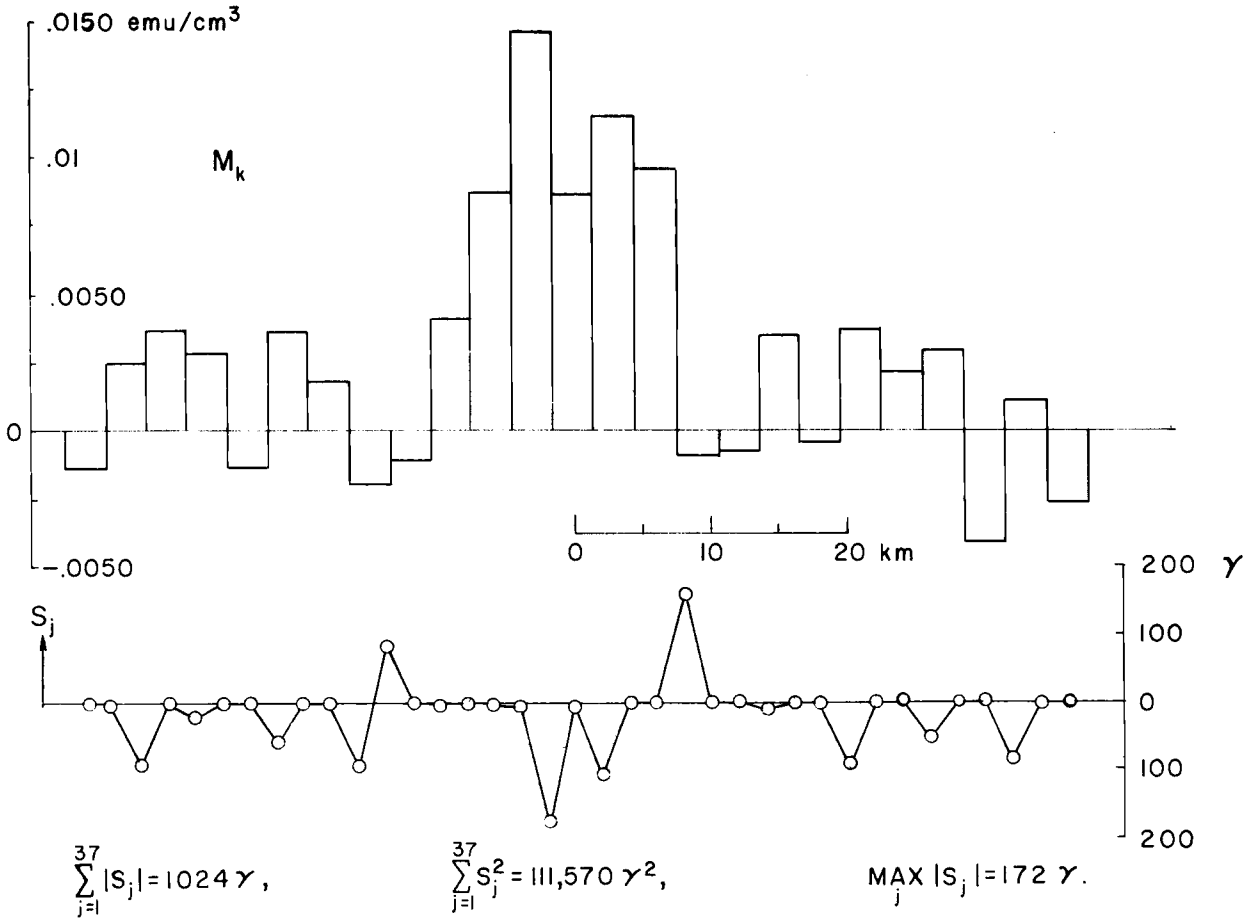

Figure 14. Magnetization values and residual field values for the n = 25 model with the L_1 norm.

$$s_j = \Delta T_j - \sum_{k=1}^{25} G_{jk} M_k.$$

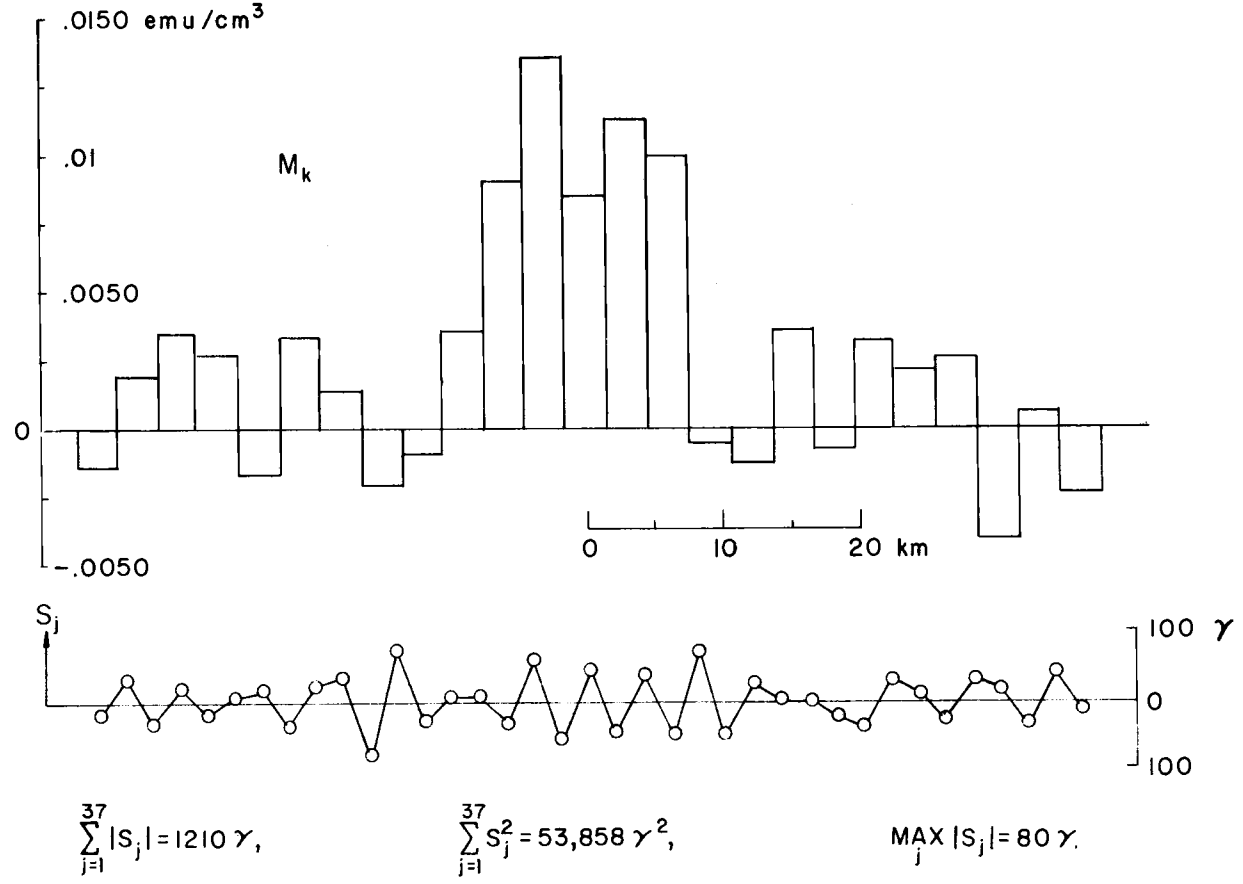

Figure 15. Magnetization values and residual field values for the n = 25 model with the L_2 norm.

$$s_j = \Delta T_j - \sum_{k=1}^{25} G_{jk} M_k.$$

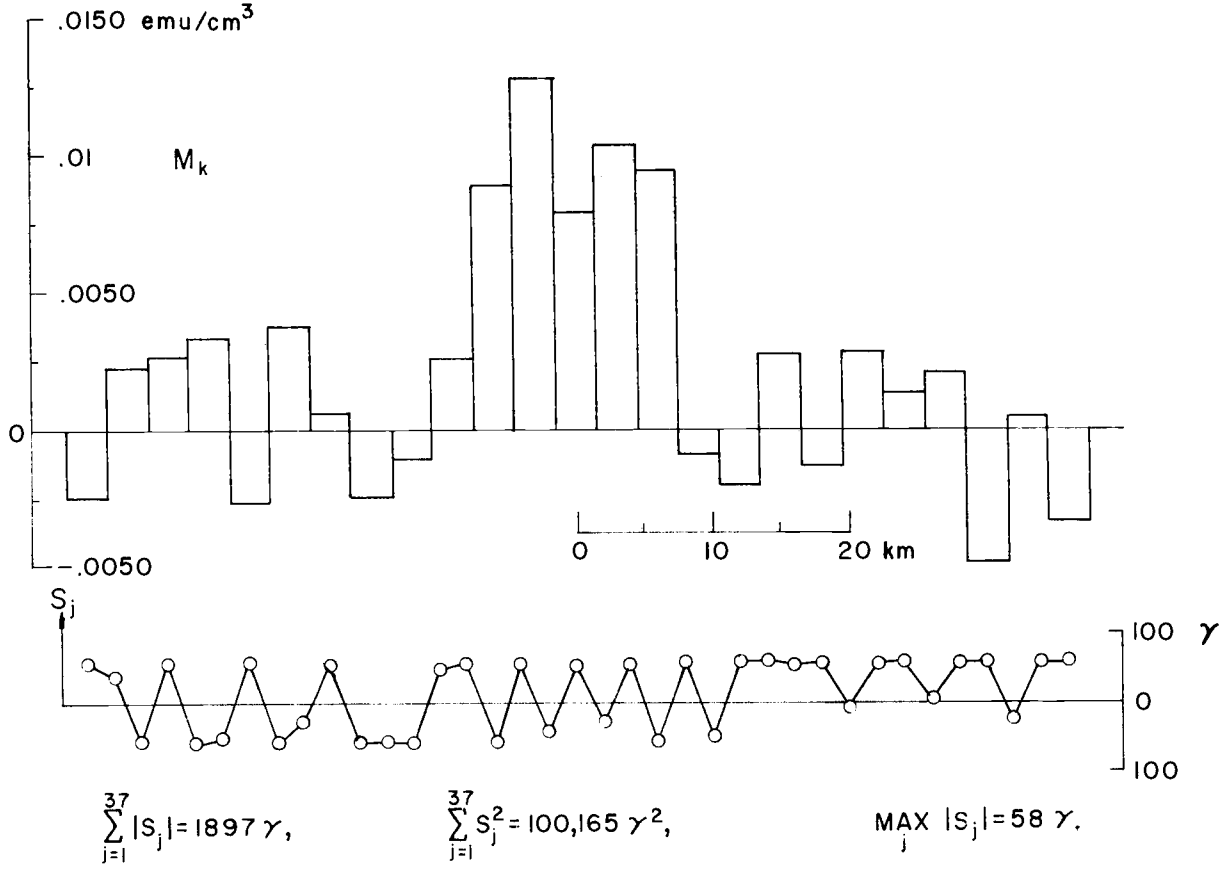

Figure 16. Magnetization values and residual field values for the n = 25 model with the L_∞ norm.

$$s_j = \Delta T_j - \sum_{k=1}^{25} G_{jk} M_k .$$

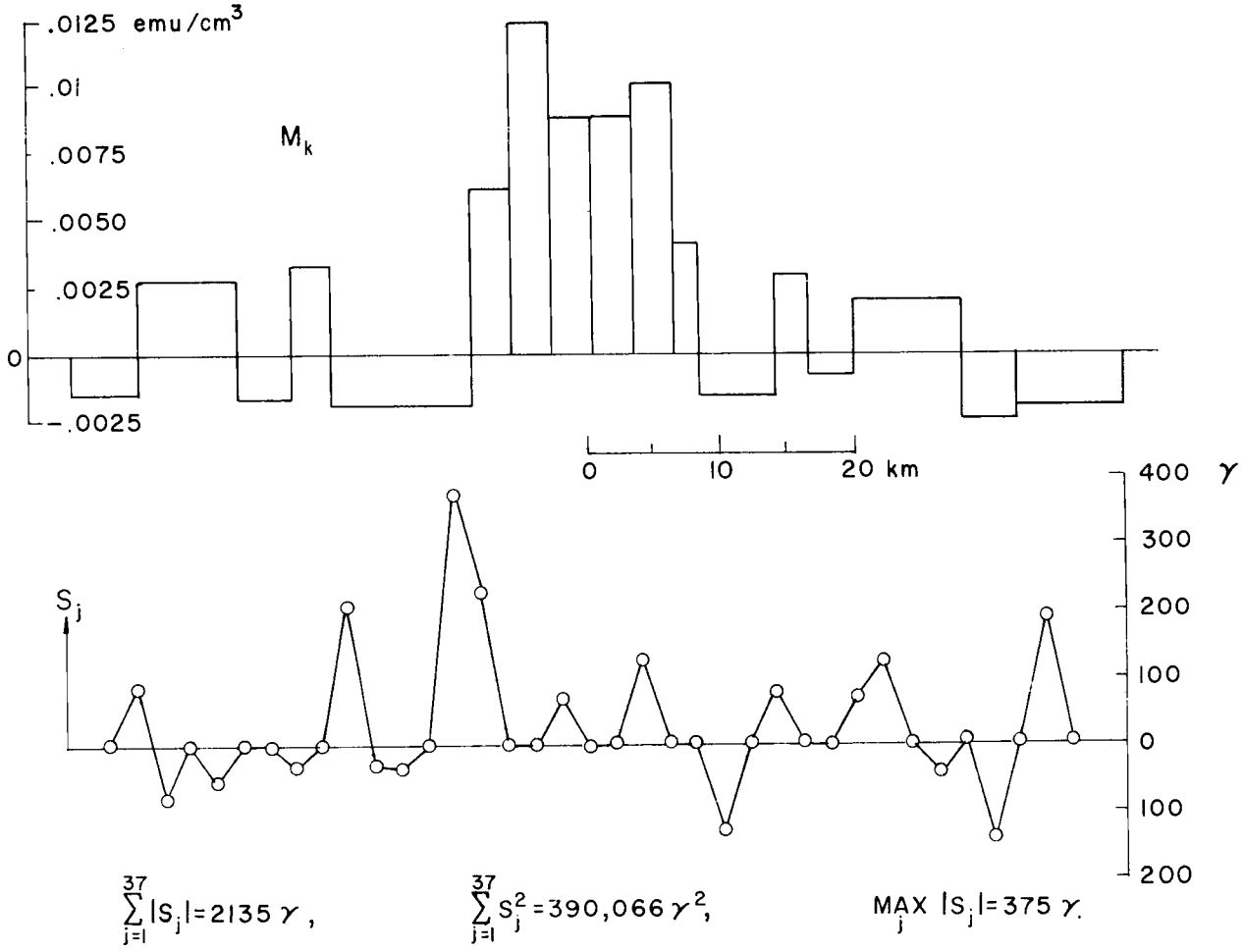

Figure 17. Magnetization values and residual field values for the n = 17 model with the L_1 norm.

$$s_j = \Delta T_j - \sum_{k=1}^{17} G_{jk} M_k .$$

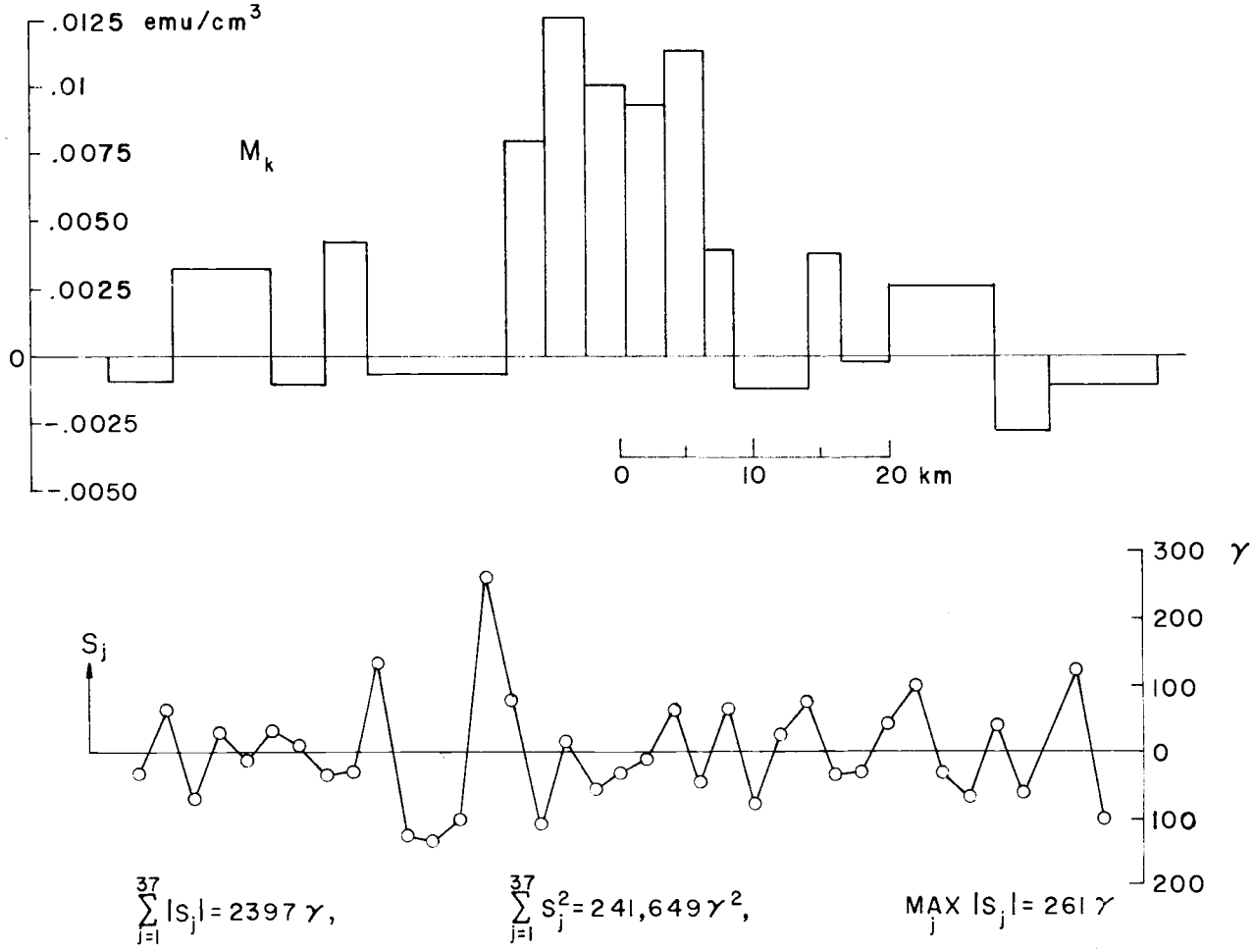

Figure 18. Magnetization values and residual field values for the n = 17 model with the L_2 norm.

$$s_j = \Delta T_j - \sum_{k=1}^{17} G_{jk} M_k.$$

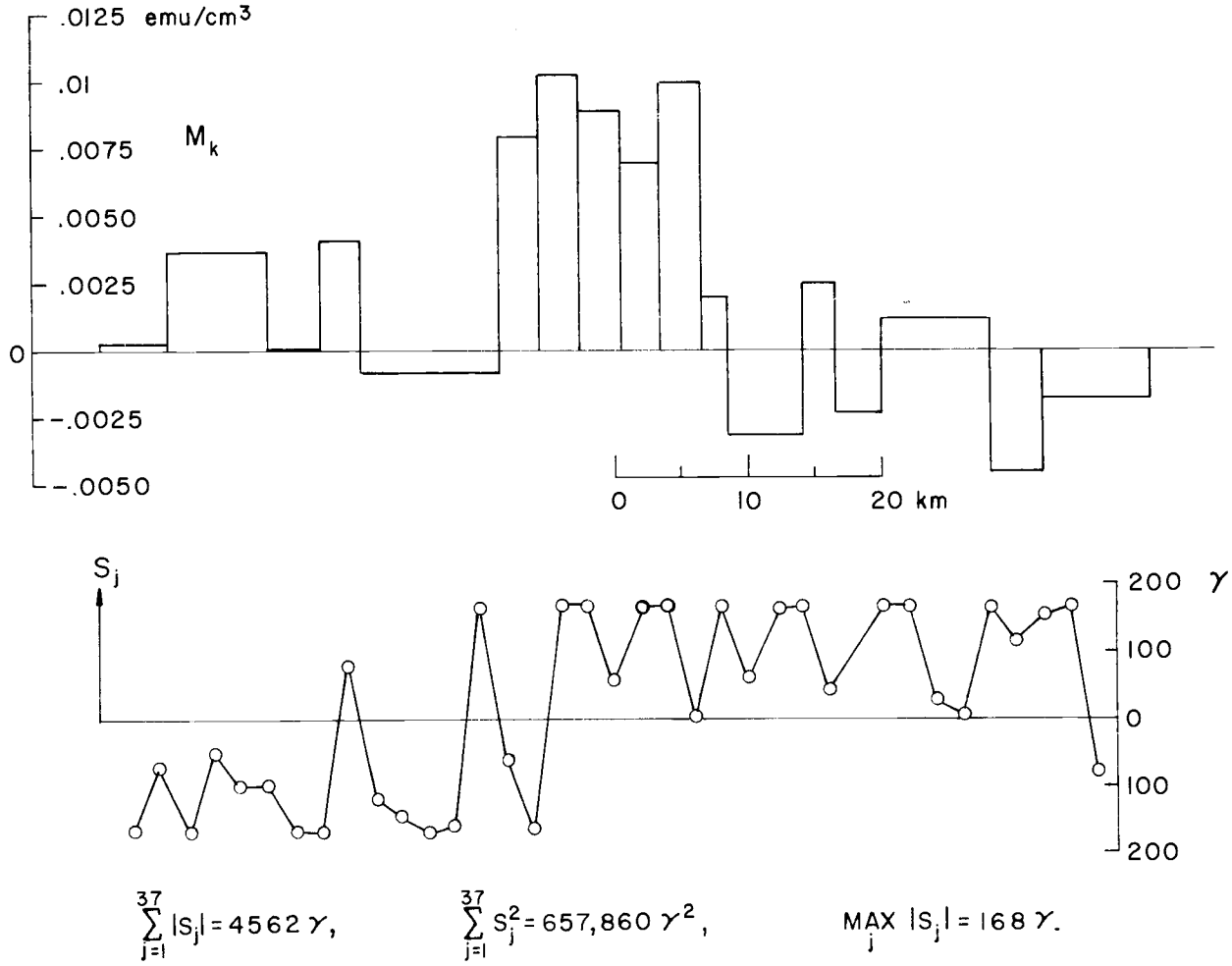

Figure 19. Magnetization values and residual field values for the n = 17 model with the L_∞ norm.

$$s_j = \Delta T_j - \sum_{k=1}^{17} G_{jk} M_k .$$

increased measurement error there. We then feel that either the L_1 or the L_2 norm is well suited to most real situations and that the L_∞ norm introduces too much error in regions of low gradient where it is not to be expected. Ultimate choice, nevertheless, depends on the purposes and characteristics of a particular investigation and on the computational properties of the various norms. As mentioned earlier, from a computational point of view the L_2 norm is found to be much more convenient than the others since it merely involves solution of a $n \times n$ system of equations.

Figure 13 presents what might be called the exact magnetization distribution, in the sense that it exactly generates the input field. But any one of the other magnetization distributions presented in Figures 14 through 19 could be considered acceptable, depending on the purposes of a particular investigation and the amount of slack that can be tolerated. This exemplifies the freedom of interpretation made possible by being able to solve the overdetermined system of equations.

CONCLUSIONS

The direct determination of the magnetization distribution in a two-dimensional source body is reduced to the problem of solving m linear algebraic equations in n unknowns:

$$\Delta T_j = \sum_{k=1}^{n} G_{jk} M_k \quad (j=1, \ldots, m)$$

where m is the number of magnetic field input points and n is the number of unknown magnetization values of n magnetic volume elements.

The case where $n = m$ can be solved uniquely provided that the system is well-conditioned (stable). That is, the dimensions of a source body should be nearly equal to the dimensions of the magnetic profile. If this is not the case the system will be ill-conditioned, and will result in a solution which will be very sensitive to slight changes in either the input field values or the matrix coefficients.

Solution of the case where $n = m$ by the iteration process is physically reasonable because with it one can obtain an approximate solution to within the experimental accuracy warranted by the experimental accuracy of the input field. That is, a sufficient magnetic model can be derived.

Magnetization distributions were obtained for two source bodies

of assumed geometry associated with ocean floor spreading. Results of the computations show that the crestal sections of the source bodies are only slightly more magnetic than their neighboring sections, and therefore these neighboring sections are very likely not extensively contaminated with material of opposite polarity. Transition zones between source-body sections of normal and reverse polarity are found to be very narrow. Therefore, they would be ineffective as sources of contamination for wide sections of normal and reverse polarity. The narrowness of the transition zones also indicates that if the dike injection hypothesis is to be accepted, then the dike injection band must be in some cases much narrower than 12 km.

Ocean floor spreading rate curves based on the usual associations of magnetic anomalies with the paleomagnetic time scale have been constructed. Two different interpretations appear possible: (1) Spreading rates have been non-uniform along the whole mid-ocean ridge system during the past 3.32 my. (2) Spreading rates have been nearly uniform; under this hypothesis, the anomaly usually associated with the Olduvai event should be associated with the Gilsa event, and another anomaly, called W, should be associated with the Olduvai event. The latter interpretation is more acceptable.

The overdetermined problem ($m > n$) has been investigated for two reasons. First, for a given number of magnetic volume elements (n) it allows improvement of the overall agreement between

the input and computed fields by an increase in the number of input points (m). Second, for a fixed number of field input points it allows the sufficiency of simpler physical models (smaller n) to be tested.

The overdetermined problem can be treated through the use of norm-functions of the deviations between the observed and computed fields. Three L_p norms were investigated: L_1, L_2, and L_∞. Of these three, the L_2 seems best suited to the problem under consideration here.

Computationally, treatment of the overdetermined problem using the L_2 norm involves the relatively simple process of solving an $n \times n$ system of linear algebraic equations. Treatment using the L_1 and L_∞ norms involves application of the complicated linear programming technique. Physically, either the L_1 norm or the L_2 norm is well suited to most real situations, while the L_∞ norm introduces too much error in regions of low gradient where only small errors are to be expected. Moreover, treatment of the overdetermined problem using the L_2 norm and the method of iteration allows the sufficiency of both the physical and the magnetic models to be considered.

BIBLIOGRAPHY

Arsac, J. 1966. Fourier transforms and the theory of distributions, tr. by A. Nussbaum and G. C. Heim. Englewood Cliffs, Prentice-Hall. 318 p.

Baker, C. T. H., L. Fox, D. F. Mayers and K. Wright. 1964. Numerical solution of Fredholm integral equations of the first kind. Computer Journal 7:141-148.

Bendat, J. S. and A. G. Piersol. 1966. Measurement and analysis of random data. New York, Wiley. 390 p.

Bott, M. H. P. 1967. Solution of the linear inverse problem in magnetic interpretation with application to oceanic magnetic anomalies. Geophysical Journal 13:313-323.

Bott, M. H. P., R. A. Smith and R. A. Stacey. 1966. Estimation of the direction of magnetization of a body causing a magnetic anomaly using a pseudo-gravity transformation. Geophysics 31:803-811.

Bullard, E. C. and R. I. B. Cooper. 1948. The determination of the masses necessary to produce a given gravitational field. Royal Society of London, Proceedings, ser. A, Mathematical and Physical Sciences 194:332-347.

Cox, A. 1968a. Assistant professor, Stanford University, Dept. of Geophysics. Personal communication. Stanford, Calif. October 5.

Cox, A. 1968b. Geomagnetic reversals. Science. (In press)

Cox, A. and G. B. Dalrymple. 1967a. Geomagnetic polarity epochs: Nunivak Island, Alaska. Earth and Planetary Science Letters 3:173-177.

Cox, A. and G. B. Dalrymple. 1967b. Statistical analysis of geomagnetic reversal data and the precision of potassium-argon dating. Journal of Geophysical Research 72:2603-2614.

Davis, J. 1968. Assistant professor, Oregon State University, Dept. of Mathematics. Personal Communication. Corvallis, Ore. July 24.

Dickson, G.O., W.C. Pitman, III and J.R. Heirtzler. 1968. Magnetic anomalies in the South Atlantic and ocean floor spreading. Journal of Geophysical Research 73:2087-2100.

Dietz, R.S. 1961. Continent and ocean basin evolution by spreading of the sea floor. Nature 190:854-857.

Doell, R.R. and G.B. Dalrymple. 1966. Geomagnetic polarity epochs: a new polarity event and the age of the Brunhes-Matuyama boundary. Science 152:1060-1061.

Doell, R.R., G.B. Dalrymple and A. Cox. 1966. Geomagnetic polarity epochs: Sierra Nevada data, 3. Journal of Geophysical Research 71:531-541.

Elsasser, W.M. 1967. Convection and stress propagation in the upper mantle. Princeton, N.J. 65 numb. leaves. (Princeton University. Dept. of Geology. Technical report no. 5, prepared under grant NsG-556 of the National Aeronautics and Space Administration)

Ewing, J. and M. Ewing. 1967. Sediment distribution on the mid-ocean ridges with respect to spreading of the sea floor. Science 156:1590-1592.

Faddeeva, V.N. 1959. Computational methods of linear algebra, tr. by C.D. Benster. New York, Dover. 252 p.

Faddeev, D.K. and V.N. Faddeeva. 1963. Computational methods of linear algebra, tr. by R.C. Williams. San Francisco, W.H. Freeman. 621 p.

Fleischer, R.L., J.R.M. Viertl, P.B. Price and F. Aumento. 1968. Mid-Atlantic Ridge: age and spreading rates. Science 161: 1339-1342.

Forsythe, G. and C.B. Moler. 1967. Computer solution of linear algebraic systems. Englewood Cliffs, N.J., Prentice-Hall. 148 p.

Fox, L. 1962. Numerical solution of ordinary and partial differential equations. Oxford, Pergammon. 509 p.

Fox, L. 1965. An introduction to numerical linear algebra. New York, Oxford University. 327 p.

Garvin, W. W. 1960. Introduction to linear programming. New York, McGraw-Hill. 281 p.

Gass, S. I. 1964. Linear programming. 2d ed. New York, McGraw-Hill. 280 p.

Grant, F. S. and G. F. West. 1965. Interpretation theory in applied geophysics. New York, McGraw-Hill. 584 p.

Gudmundsson, G. 1966. Interpretation of one-dimensional magnetic anomalies by use of the Fourier-transform. Geophysical Journal. 12:87-97.

Hadley, G. 1964. Nonlinear and dynamic programming. Reading, Mass., Addison-Wesley. 484 p.

Harrison, C. G. A. 1968. Formation of magnetic anomaly patterns by dyke injection. Journal of Geophysical Research 73:2137-2142.

Heirtzler, J. R., G. O. Dickson, E. M. Herron, W. C. Pitman, III and X. Le Pichon. 1968. Marine magnetic anomalies, geomagnetic field reversals, and motions of the ocean floor and continents. Journal of Geophysical Research 73:2119-2136.

Heirtzler, J. R., X. Le Pichon and J. G. Baron. 1966. Magnetic anomalies over the Reykjanes Ridge. Deep-Sea Research 13: 427-443.

Heirtzler, J. R., G. Peter, M. Talwani and E. G. Zurflueh. 1962. Magnetic anomalies caused by two-dimensional structure: their computation by digital computers and their interpretation. 63 numb. leaves. (Columbia University. Lamont Geological Observatory. Technical report no. 6. On Contract CU-6-62 Nonr-Geology)

Herron, E. M. and J. R. Heirtzler. 1967. Sea-floor spreading near the Galapagos. Science 161:775-780.

Hess, H. H. 1965. Mid-oceanic ridges and tectonics of the sea-floor. In: Submarine geology and geophysics, ed. by W. F. Whittard and R. Bradshaw. London, Butterworths. p. 317-332. (Colston Papers no. 17)

Isacks, B., J. Oliver and L. R. Sykes. 1968. Seismology and the new global tectonics. Journal of Geophysical Research 73: 5855-5899.

Knopoff, L. 1964. The convection current hypothesis. Reviews of Geophysics 2:89-122.

Kreisel, G. 1949. Some remarks on integral equations with kernals: $L(y_1-x_1, \ldots, y_n-x_n;a)$. Royal Society of London, Proceedings, ser. A, Mathematical and Physical Sciences 197:160-183.

Larson, R. L., H. W. Menard and S. M. Smith. 1968. Gulf of California: a result of ocean-floor spreading and transform faulting. Science 161:781-784.

Lee, Y. W. 1960. Statistical theory of communication. New York, Wiley. 509 p.

Le Pichon, X. 1968. Sea-floor spreading and continental drift. Journal of Geophysical Research 73:3661-3697.

Le Pichon, X. and J. R. Heirtzler. 1968. Magnetic anomalies in the Indian Ocean and sea-floor spreading. Journal of Geophysical Research 73:2101-2117.

Loncarevic, B. D., C. S. Mason and D. H. Matthews. 1966. Mid-Atlantic Ridge near 45° North. I. The median valley. Canadian Journal of Earth Sciences 3:327-349.

MacDonald, G. J. F. 1965. Continental structure and drift. In: A symposium on continental drift, organized by P. M. S. Blackett, E. Bullard and S. K. Runcorn. London, The Royal Society. p. 215-227.

McDougall, I. and H. Wensink. 1966. Paleomagnetism and geochronology of the Pliocene-Pleistocene lavas in Iceland. Earth and Planetary Science Letters 1:232-236.

Mason, R. G. 1958. A magnetic survey off the west coast of the United States between latitudes 32° and 36° N, longitudes 121° and 128° W. Geophysical Journal 1:320-329.

Mason, R. G. and A. D. Raff. 1961. Magnetic survey off the west coast of North America, 32° N. latitude to 42° N. latitude. Geological Society of America, Bulletin 72:1259-1266.

Morgan, W. J. 1968. Rises, trenches, great faults, and crustal blocks. Journal of Geophysical Research 73:1959-1982.

Nettleton, L. L. 1954. Regionals, residuals, and structures. Geophysics 19:1-22.

Ozima, M., M. Ozima and I. Kaneoka. 1968. Potassium-argon ages and magnetic properties of some dredged submarine basalts and their geophysical implications. Journal of Geophysical Research 73:711-723.

Peters, L. J. 1949. The direct approach to magnetic interpretation and its practical application. Geophysics 14:290-320.

Phillips, D. L. 1962. A technique for the numerical solution of certain integral equations of the first kind. Association for Computing Machinery, Journal 9:84-97.

Phillips, J. D. 1967. Magnetic anomalies over the Mid-Atlantic Ridge near 27° N. Science 157:920-922.

Pitman, W. C., III and J. R. Heirtzler. 1966. Magnetic anomalies over the Pacific-Antarctic Ridge. Science 154:1164-1171.

Pitman, W. C., III, E. M. Herron and J. R. Heirtzler. 1968. Magnetic anomalies in the Pacific and sea floor spreading. Journal of Geophysical Research 73:2069-2085.

Rabinowitz, P. 1968. Applications of linear programming to numerical analysis. SIAM Review 10:121-159.

Raff, A. D. and R. G. Mason. 1961. Magnetic survey off the west coast of North America, 40° N. latitude to 52° N. latitude. Geological Society of America, Bulletin 72:1267-1270.

Rice, J. R. 1964. The approximation of functions. Reading, Mass., Addison-Wesley. 203. p.

Rice, J. R. and J. S. White. 1964. Norms for smoothing and estimation. SIAM Review 6:243-256.

Scheurman, L. H. 1968. Instructor, Oregon State University, Computer Center. Personal communication. Corvallis, Ore. September 16.

Smellie, D. W. 1956. Elementary approximations in aeromagnetic interpretation. Geophysics 21:1021-1040.

Smith, R. A. 1959. Some depth formulae for local magnetic and gravity anomalies. Geophysical Prospecting 7:55-63.

Smith, R. A. 1961. Some theorems concerning local magnetic anomalies. Geophysical Prospecting 9:399-410.

Talwani, M. and J. R. Heirtzler. 1964. Computation of magnetic anomalies caused by two dimensional structures of arbitrary shape. In: Computers in the mineral industries, ed. by G. A. Parks et al. Proceedings of the Third Annual Conference, Stanford, Calif., 1963. Stanford. p. 464-480. (Stanford University Publications, Geological Sciences. Vol. 9, no. 1)

Tanner, J. G. 1967. An automated method of gravity interpretation. Geophysical Journal 13:339-347.

Tarling, D. H. 1966. The magnetic intensity and susceptibility distribution in some Cenozoic and Jurassic basalts. Geophysical Journal 11:423-432.

Turing, A. M. 1948. Rounding-off errors in matrix processes. Quarterly Journal of Mechanics and Applied Mathematics 1:287-308.

Vacquier, V., A. D. Raff and R. E. Warren. 1961. Horizontal displacements in the floor of the northwestern Pacific Ocean. Geological Society of America, Bulletin 72:1251-1258.

Vacquier, V., N. C. Steenland, R. G. Henderson and I. Zietz. 1951. Interpretation of aeromagnetic maps. New York. 151 p. (Geological Society of America. Memoir 47)

Vajda, S. 1961. Mathematical Programming. Reading, Mass., Addison-Wesley. 310 p.

van Andel, T. J. 1968. The structure and development of rifted mid-oceanic rises. Journal of Marine Research 26:144-161.

Vine, F. J. 1966. Spreading of the ocean floor: new evidence. Science 154:1405-1415.

Vine, F. J. and D. H. Matthews. 1963. Magnetic anomalies over ocean ridges. Nature 199:947-949.

Vine, F. J. and J. Tuzo Wilson. 1965. Magnetic anomalies over a young oceanic ridge off Vancouver Island. Science 150:485-489.

Watkins, N. D. and H. G. Goodell. 1967. Confirmation of the reality of the Gilsa geomagnetic polarity event. Earth and Planetary Science Letters 2:123-129.

APPENDIX

Linear Programming

In this appendix a brief survey of the general linear programming (LP) formulation is presented along with some pertinent theorems and definitions. Excellent sources of information on LP are Garvin (1960), Gass (1964), and Vajda (1961).

Linear programming is a method of solving an indeterminate system of linear equations in which the variables must be non-negative and must conform to an additional linear extremal condition. More precisely, it solves the system

$$(1) \qquad \sum_{k=1}^{n} a_{jk}x_k = b_j \quad (j=1,\ldots,m)$$

with

$$(2) \qquad x_k \geq 0,$$

$$(3) \qquad \sum_{k=1}^{n} c_k x_k = \min,$$

and where a_{jk}, b_j, and c_k are known constants for all values of j and k. Equations (1) are called the constraints of the problem and the left side of Equation (3) is called the objective function. The above system is the standard LP problem where the constraints are represented as equations, all the variables are required to be

non-negative, and where the objective function is to be minimized.

If some variables in the physical problem are not required to be non-negative, then the variables can be expressed in two different ways; that is

$$x_k = x_k^+ - x_k^- \quad \text{with} \quad x_k^+ \geq 0, \quad x_k^- \geq 0$$

(4) or

$$x_k = z_k - C \quad \text{with} \quad z_k \geq 0, \quad C = \text{constant}.$$

The first of these has the rather distinct disadvantage of changing one variable into two variables, thus greatly increasing the size of problems where many of the original variables may be positive or negative (this is the case in problems considered here where all the original magnetization variables are unconstrained in sign). On the other hand, the second form does not increase the number of variables.

In some cases the computations may be shortened through use of the dual of the original or primal problem. If the primal problem is denoted as

$$\sum_{k=1}^{n} a_{jk} x_k \geq b_j \quad (j=1, \ldots, m),$$

$$\sum_{k=1}^{n} c_k x_k = z = \min, \quad x_j \geq 0$$

then the dual problem is obtained by transposing the rows and columns of these equations, including the right hand side and the objective function, reversing the inequalities, and maximizing instead of minimizing. Thus

$$\sum_{j=1}^{m} a_{jk} y_j \leq c_k \quad (k = 1, \cdots, n),$$

$$\sum_{j=1}^{m} b_j y_j = v = \max,$$

$$y_j \geq 0$$

is the dual problem and the y_i's are the dual variables. If the solution to this dual problem is known, then the solution to the primal problem follows; these solutions are usually given together. Use of the dual may be helpful in reducing computation time when $m > n$ because the primal problem has m constraints whereas the dual has n constraints (the number of constraints is much more important than the number of variables in determining computation time, (Rabinowitz, 1968).

Important theorems concerning the dual (Garvin, 1960, Chapter 17) follow:

(a) The dual of the dual is the primal.

(b) If the kth constraint of the primal is an equality, then the

dual variable y_k is unrestricted in sign.

(c) If the pth variable of the primal is unrestricted in sign, the pth constraint of the dual is an equality.

It should be mentioned here that the LP method allows placement of an upper bound on the variables. Equation (2) would then become $0 \leq x_k \leq \text{U.B.}$, where U.B. means upper bound. For the case where x_k is unrestricted in sign, and both upper and lower bounds are to be considered, the second of Equations (4) is more versatile. It can be written

$$x_k = z_k - C, \quad 0 \leq z_k \leq \text{U.B.}$$

which means that for the original problem

$$-C \leq x_k \leq \text{U.B.} - C,$$

that is, the lower bound does not have to equal the upper bound.